University of Alberta

Characterization of Particulate Emissions of Homogeneous Charge Compression Ignition Engines

by

Dallin Scott Bullock

A thesis submitted to the Faculty of Graduate Studies and Research
in partial fulfillment of the requirements for the degree of

Master of Science

Mechanical Engineering

Fall 2013
Edmonton, Alberta

Abstract

The particle size distribution, volatility, and effective density of particulate matter are measured using a cooperative fuel research engine during motoring, spark ignition, and homogeneous charge compression ignition. For all operating modes, less than 5% of the particulate mass remains when denuding the sample at 100 °C, and the particles for each operating mode have a relatively constant density with respect to particle size.

A single cylinder engine with electromagnetic valves is used to test the effect of changing valve timing on particle emissions. An order of magnitude increase in particle concentration coincides with the valve timing changes, whereas the geometric mean diameter remains constant, suggesting that while the particle concentration increases due to timing changes, the mechanism for particle formation does not change. After a spike in particle concentration due to a timing change, the value quickly returns to steady-state levels.

Acknowledgments

I would like to express thanks to my supervisor Dr. Jason Olfert for his encouragement and support throughout this research. He has been a great supervisor who was helped me to accomplish my goal. I would also like to thank my co-supervisor Dr. David Checkel for affording me this opportunity.

I would also like to thank Rick Conrad and Bernie Faulkner for their assistance with the seemingly endless troubleshooting that was required in order for me to complete my research.

The great opportunity to work alongside colleagues Jason Boddez, Dan Handford, Michael Schleppe, Masoud Mashkournia, Alex Schramm, Tyler Johnson, and Ali Momenimovahed has provided me with help and assistance for which I am sincerely grateful.

Lastly, the love and support of my family is what truly made this possible. Without my parents, siblings, close friends, and especially my wife, I could not have succeeded.

Table of Contents

List of Tables

List of Figures

Nomenclature

Acronyms

APM	Aerosol Particle Mass Analyzer
CCN	Cloud Condensation Nuclei
CDNC	Cloud Droplet Number Concentration
CFR	Cooperative Fuels Research
CH_4	Methane
CI	Compression Ignition
CNG	Compressed Natural Gas
CO_2	Carbon Dioxide
CPC	Condensation Particle Counter
CPMA	Centrifugal Particle Mass Analyzer
CR	compression ratio
CVS	Constant Volume Sampler
DMA	Differential Mobility Analyzer
DMS	Differential Mobility Spectrometer
EC	European Commission
EGR	Exhaust Gas Recirculation

E_n	Electrometer rings of DMS
EU	European Union
GMD	Geometric Mean Diameter
GPMS	Golden Particle Measurement System
GSD	Geometric Standard Deviation
H_2O	Water
HCCI	Homogeneous Charge Compression Ignition
HEPA	High Efficiency Particulate Air
HRV	Heart Rate Variability
IMEP	Indicated Mean Effective Pressure
JRC	Joint Research Centre
LEPA	Low Efficiency Particulate Air
LWC	Liquid Water Content
M	Total Particle Mass
N	Total Particle Number
NOx	Nitrous Oxides
NVO	Negative Valve Overlap
O_2	Diatomic Oxygen

PM	Particulate Matter
PMP	Particulate Measurement Programme
PN	Particulate Number
PNC	Particle Number Counter
PND	Particle Number Diluter
PRBS	Pseudo Random Binary Signal
rpm	Revolutions Per Minute
SAE	Society of Automotive Engineers
SI	Spark Ignition
SMPS	Scanning Mobility Particle Spectrometer
VPR	Volatile Particle Remover

Symbols

C_C	Slip Correction Factor
$dN/d\log d_p$	Normalized Concentration (cm^{-3})
d_p	Particle Diameter (nm)
d_m	Particle Mobility-Equivalent Diameter (nm)
e	Charge of an Electron (1.602×10^{-19} C)
E	Electrical Field (V/m)
F_c	Centrifugal Force (N)
F_d	Drag Force (N)
F_e	Electrical Force (N)
V	Velocity (m/s)
μ	Viscosity (kgm/s)
ω_1	Angular velocity of inside cylinder of CPMA (rad/s)
ω_2	Angular velocity of outside cylinder of CPMA (rad/s)
T_{exh}	Exhaust Temperature
Φ	Equivalence Ratio

Chapter 1: Introduction to Particulate Emissions

In Homogenous Charge Compression Ignition (HCCI), a fully mixed dilute fuel and air mixture is drawn into the cylinder. By using a high compression ratio and/or a high intake temperature, the charge is able to auto-ignite. With this combination of homogeneous charge and high compression ratio, HCCI can provide significant improvements in both efficiency and emissions over that of conventional internal combustion engines. Engine efficiency is improved with increased compression ratio (Heywood, 1988; Zhao, 2007). The homogeneous charge prevents a region of rich combustion, which reduces the formation of solid particles (Li, 2007). Often, in HCCI engines, the peak in-cylinder combustion temperature is lower due to a dilute mixture, and this results in much lower levels of nitrous oxides (Li, 2007; Stanglmaier, 2001). A comparison of spark ignition (SI), compression ignition (CI), and HCCI engines is shown in Figure 1.1.

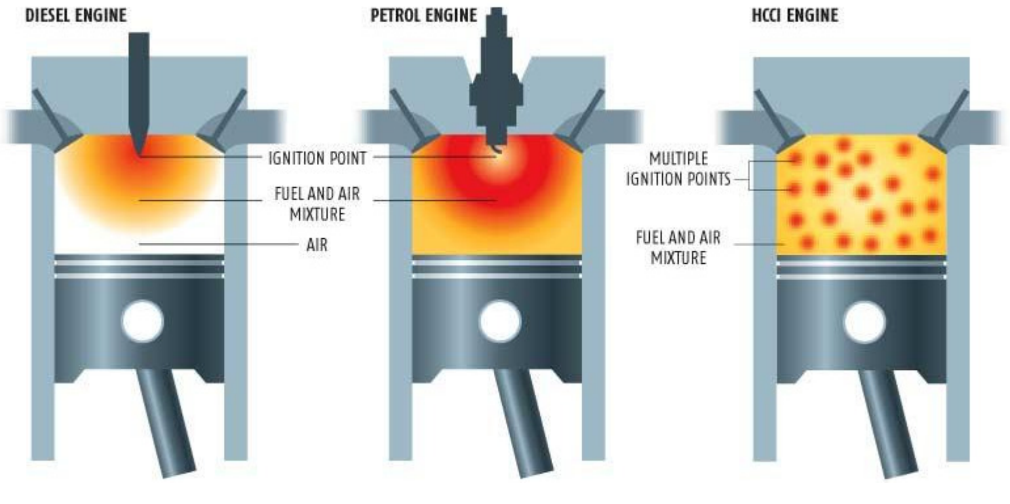

Figure 1.1: In diesel or CI engines, the fuel is injected into the cylinder causing areas of rich and lean burn. In petrol or SI engines, flame propagation results in higher combustion temperatures and pressures in comparison to HCCI (Marshall, 2006)

Because of the relatively new combustion strategy of HCCI, very little research has been done to investigate the resulting particulate matter (PM) emissions.

1.1 Particulate Emission Properties

Engine emissions contain both gas-phase and particulate matter. PM emissions can be divided into three different modes that are formed in distinct ways. Figure 1.2 shows the typical PM size distribution with respect to both size and mass. This demonstrates that while small particles don't have much mass, the high number concentration may be harmful, and are therefore important. The smallest mode has particle diameters of approximately 50 nm or less, and is referred to as the nucleation mode. These particles are formed as gas-phase material condenses to form solid or liquid PM. Particles in the nucleation mode undergo rapid growth as more material coagulates (Hinds, 1999).

Once these particles grow to approximately 0.1 μm, they enter the accumulation mode. Typically, solid particles begin to stick together into larger agglomerates to form large, non-spherical particles (Eastwood p. 43, 2008).

Coarse particles (generally greater than 2.5 μm) have a much denser solid core than accumulation mode particles, and may contain an outer layer of volatile particles. These particles may form over a longer period of time; often from particles that deposit in the exhaust system, form into larger particles, and then become airborne again (Eastwood p. 42, 2008). While this is one mechanism for the formation of coarse mode particles, they are most often formed by mechanical means (Hinds, 1999).

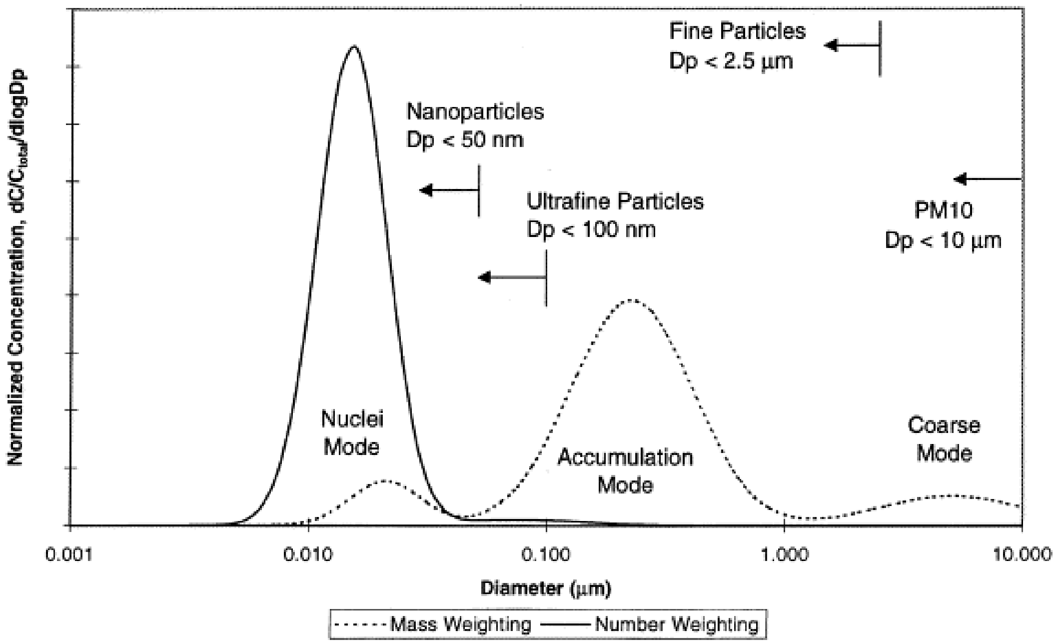

Figure 1.2: Typical engine exhaust size distribution with respect to number and mass (Kittelson, 1998).

PM emissions consist of many types of compounds, but can be simplified into solid and volatile compounds. The solid compounds are mainly composed of carbonaceous material, otherwise known as soot, which is elemental carbon. Soot is primarily formed when incomplete combustion takes place in locally fuel-rich regions inside the cylinder (Eastwood p. 62, 2008).

The volatile fraction of the PM consists mostly of organic compounds and sulphates. However, modern fuels have significantly lower sulfur content, greatly reducing the amount of sulphates present (Eastwood p. 122, 2008). The major source of the organic fraction is fuel that has not been fully oxidized. Some fuel usually remains unburned near the threads of the spark plug or in the gap between the piston and the cylinder wall and can also result from incomplete combustion due to locally rich or locally lean regions within the cylinder (Heywood, 1998). Another source of organic PM comes from gas-to-particle conversion, which is the condensation of gas-phase hydrocarbons. More volatile fuels are less susceptible to gas-to-particle conversion (Eastwood p. 321, 2008).

However, it has been suggested that fuel is not the only source of the organic fraction (Kayes and Hochgreb, 1999) and that unburned fuel could even be the smaller component (Shin and Cheng, 1997) in comparison to lubricating oil.

Diesel engines are most commonly known for the production of soot. In fact, they operate in a manner similar to the industrial manufacturing of black carbon (Lockwood and van Niekerk, 1995; Taylor, 1997). The production of soot is mainly due to fuel-rich regions caused by combustion during insufficient mixing within the cylinder (Eastwood p. 321, 2008). However, while diesel vehicles do produce significant amounts of soot, Kleeman et al (2000) showed that particles emitted from diesel vehicles also contained significant amounts of organic compounds. In diesel engines, it has been shown that lubricating oil can be the majority of organic compounds present in the PM (Munro, 1990).

Kleeman et al (2000) also showed that particles emitted from port injection gasoline vehicles were largely composed of organic carbon, as opposed to elemental carbon. And while there is some soot emitted from these engines, they are quite low as long as the engine is properly tuned and maintained (Quader, 1989).

With direct injection, the fuel has less time to fully mix with the air and as a result the charge is more stratified. This creates fuel-rich regions within the cylinder, which encourage the formation of soot (Yang and Kenney, 2002). Also, because the fuel is injected directly into the cylinder before combustion occurs, fuel tends to wet the piston surface (Karlsson and Heywood, 2001). Once the liquid fuel on the surface of the piston ignites, it is long-burning and highly sooting (Mehta et. al., 2001). The wetting of the piston surface can also contribute to increased hydrocarbon emissions, some of which will undergo gas-to-particle conversion and result in organic particulates (Huang et. al., 2001a).

1.2 Climate Change

Particles in the atmosphere have been shown to affect climate. One such effect is from the scattering and absorption of light. By scattering light, the amount of solar energy trapped in the atmosphere is decreased, causing a cooling effect, whereas by absorbing light, the amount of solar energy trapped in the atmosphere is increased, causing a warming effect. Particles will both scatter and absorb, but which effect is greater depends on the size, morphology, and composition of the particle (Kokhanovsky, 2008). Light scattering is mostly determined by the particle size and shape. Larger particles scatter the most light, whereas ultrafine and nanoparticles scatter very little light (Kittelson, 1998). Absorption on the other hand is closely related to the carbon content of the particles (Kittelson, 1998) and therefore soot, like that from diesel engines, mostly absorbs light (Horvath, 1993). Ramanathan (2008) also showed that decreasing soot in the atmosphere could decrease global warming.

Particles can also have indirect effects on climate through changing the properties of clouds. The particles in the atmosphere act as cloud condensation nuclei, and therefore, a greater particle concentration will result in clouds forming with a greater number of smaller droplets. Because of this, the cloud will scatter more light contributing to a global cooling effect. This is known as the “cloud albedo effect” (Remer, 2007). In addition to changing the scattering properties of the cloud, the decrease in droplet size lengthens the lifetime of clouds by preventing precipitation. This will also have a negative radiative forcing effect (Penner, 2001). A summary of these effects is shown in Figure 1.3.

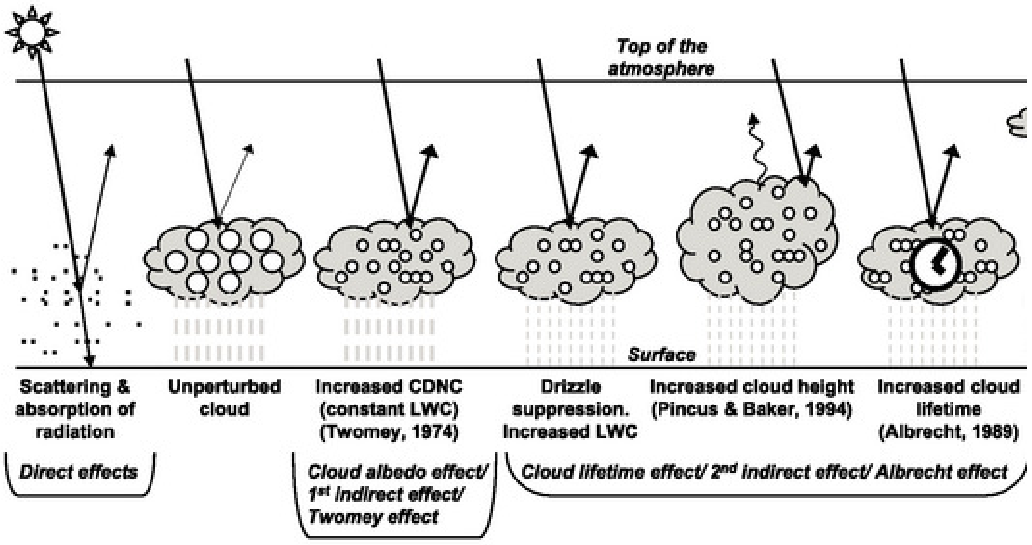

Figure 1.3: A summary of the different radiative forcing mechanisms in relation to PM. The black dots represent particles; the open circles represent water droplets. Straight lines represent solar radiation. Cloud droplet number concentration (CDNC), liquid water content (LWC) and cloud condensation nuclei (CCN) have been abbreviated. (Modified from IPCC, 2007)

1.3 Health Effects

Human health can also be affected by particles. This has been suggested as far back as the 1980's, and has been the subject of many studies; a review of which was done by Pope III (2000). It is also important to note that while most studies have focused on particle mass, the deposition efficiency in the human respiratory tract suggests that particle size is more important (International Commission on Radiological Protection, 1966) and that the correlation between health effects and particle concentration is improved when a fine particle concentration (<2.5 microns) is used (Dockery, 1993; Pope III, 1995). It has been shown that exposure to high concentration of PM can cause nausea, difficulty breathing, cancer, early death, and cardiopulmonary mortality and that the respiratory, cardiovascular, nervous, urinary, and digestive systems can all be affected (Kampa, 2008). In 2005, Schwartz, showed that there is also a relation between particle concentration and heart rate variability (HRV), which is a risk factor for sudden death.

Pope III (2002) has suggested that long-term exposure may show an even greater correlation between particle concentration and health effects.

1.4 Visibility

The scattering and absorption of light also reduces visibility, which is defined as the distance at which an object is only barely visible (Hinds, 1999). Particles are the greatest factor in light scattering and absorption; responsible for 90% in rural areas and 99% in urban areas (Horvath, 1994). In a study by Eidels-Dubovoi (2002), it was shown that the average visibility in downtown Mexico City was 20.9 km, as opposed to 30.3 km in a suburban area.

1.5 Regulations

PM regulations have been in place in the European Union for diesel vehicles since the early 1990's (Euro 1). At that time, only the mass of the PM was regulated. These measurements are done by using a filter to collect all PM from the engine exhaust and then weighing the filter to determine the mass of PM collected. These regulations also came to gasoline vehicles in 2009. (Euro 5).

In 2011 (2014 for gasoline vehicles) (Euro 5/6), the EU also added a particle number emission limit. A summary of the European PM emission regulations is shown in Table 1.1.

Table 1-1: PM regulations for diesel and gasoline engines. Data taken from Euro 1/2/3/4/5/6. M represents particle mass, and N represents particle number.

EU Emission Standards for Passenger Cars

Stage	Date	CI (Diesel)		SI (Gasoline)	
	(Year.Month)	M (g/km)	N (km^{-1})	M (g/km)	N (km^{-1})
Euro 1	1992.07	0.14	-	-	-
Euro 2	1996.01	0.08	-	-	-
Euro 3	2000.01	0.05	-	-	-
Euro 4	2005.01	0.025	-	-	-

Euro 5a	2009.09	0.005	-	0.005	-
Euro 5b	2011.09	0.005	6E+11	0.005	-
Euro 6	2014.09	0.005	6E+11	0.005	6E+11

While the particle mass regulations are measured on the basis of all PM in the exhaust sample, particle number regulations are based on solid particles. This means that a method must be used to remove all volatile material before the particle count is recorded. The measurement procedure references the Particulate Measurement Programme (PMP Joint Research Centre, 2007). Figure 1.4 below shows a schematic of the number measurement system.

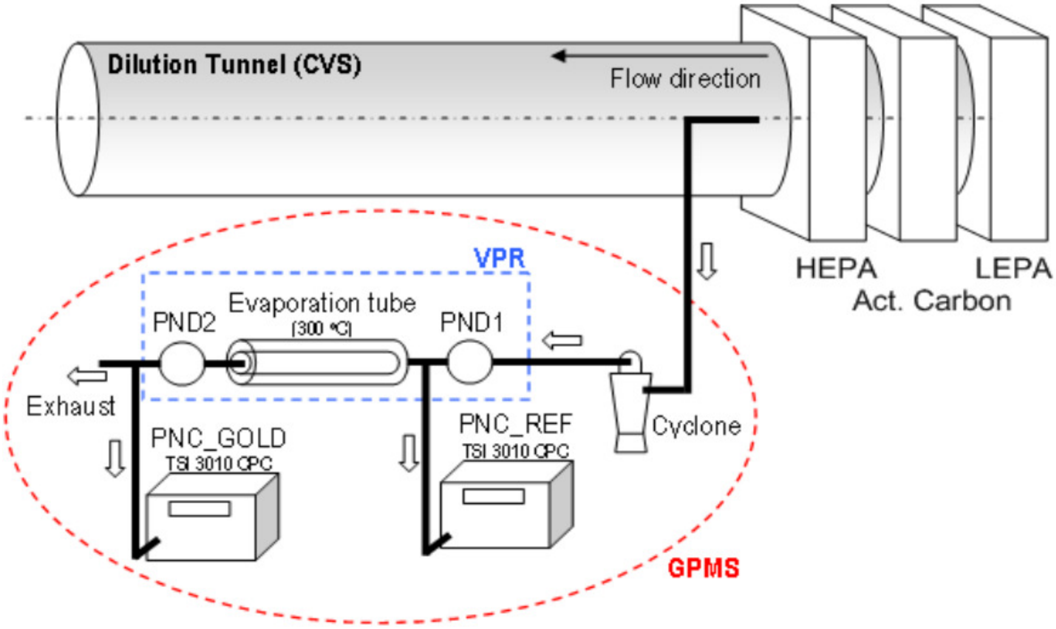

Figure 1.4: From European Commission JRC, 2007.

First, the emissions are sampled from a dilution tunnel using a probe and are passed through a cyclone to eliminate any particles larger than 2.5 μm. The sample then passes through the first particle number diluter (PND1) and is heated to 150 °C to evaporate volatile particles. The sample is then heated to 300°C to evaporate any semi-volatile particles. This ensures that all remaining particles are solid. After this, the sample is passed through a second diluter (PND2), which causes the sample to be cooled, and the concentration of evaporated material is decreased so that it will not recondense on the solid particles or nucleate. The particle number counter (PNC_GOLD) then measures the concentration of the particles. A nominal lower limit of 23 nm is set to exclude possible nucleated hydrocarbons.

1.6 Previous Research on HCCI Particulate Emissions

PM emissions from HCCI combustion have often been assumed to be negligible. Gray et al(1997), however, measured the HCCI particulate emissions with diesel fuel, and concluded that they were considerable, and were due to the presence of long-chain hydrocarbons in the fuel. Gray measured the particulate emissions present for HCCI combustion of both diesel fuel and blended hexadecane/heptane. Compared to direct injection diesel, HCCI showed a 27% reduction in particulates. Gray also saw a strong dependence of PM emissions on intake air temperature.

Price (2007) showed that for gasoline direct injection, HCCI had slightly higher particle concentrations than for SI, and had fairly similar size distributions. A large accumulation mode of mean diameter between 80 and 100 nm was present. Price showed that the accumulation mode particle concentration decreased with increasing exhaust gas recirculation (EGR). A smaller nucleation mode of mean diameter between 10 and 20 nm was also present.

Kaiser (2005) measured the HCCI PM resulting from gasoline combustion for a range of air/fuel ratios from 50 to 230. For air-fuel ratios of less than 70, the particulate emissions were characteristic of soot emissions, whereas for air-fuel ratios of greater than 70, a sharp change to semi-volatile particle characteristics was observed.

Agarwal (2013) performed diesel HCCI combustion with varying EGR and air-fuel ratios. It was shown that increased air-fuel ratio (more lean), as well as increased EGR, resulted in increased organic fraction. The size distribution was also measured, along with the morphology of collected particles using scanning electron microscopy.

Franklin (2010) showed that for both ethanol and hydrogen fuel, and for multiple engine loads, the PM distributions were essentially free of accumulation mode particles. Nucleation mode particles were present in significant mass and number. An analysis of particle volatility provided evidence suggesting that the PM was primarily lubricating oil. This, combined with lubricating oil consumption, suggested that the PM from HCCI was formed by gas-to-particle conversion of the lighter distillates from the lubricating oil.

1.7 Purpose of this work

The purpose of this work is to better understand the physical properties of PM resulting from motoring, SI, and HCCI. These physical properties include size, concentration, volatility, and density and were measured using a CFR engine, along with a DMS, CPC, denuder, and CPMA. Understanding these properties is important in order to meet current and upcoming automotive PM regulations, which give limits for the particle mass as well as the non-volatile particle number.

By comparing the particulate emissions of motoring, SI, and HCCI, as well as compression ratio and power level effects, an investigation of the formation mechanisms for particulate emissions is possible. Knowing the effect of these parameters on PM emissions, as well as how the particles are formed, allows strategies for further reductions of engine particulate emissions to be developed. Engine manufacturers will be able to determine the best way to eliminate the specific particles formed.

Measuring the effects of transient engine operation on particulate emissions allows for a clearer picture of the total PM produced by HCCI combustion in the real world. Also, by comparing the particle size distributions to those of steady-state operation, any change in composition during transient operation can be detected. This was accomplished with a single-cylinder engine fitted with fully-variable electromagnetic valves and a fast-response DMS.

1.8 References

Agarwal, A., K., Singh, A. P., Lukose, J., Gupta, T. (2013). Characterization of exhaust particulates from diesel fueled homogenous charge compression ignition combustion engine. *Journal of Aerosol Science*, 58: 71-85.

Dockery, D. W., Pope III, A., Xu, X., Spengler, J. D., Ware, J. H., Fay, M. E., Ferris, Jr. B. G., Speizer, F. E. (1993). An association between air pollution and mortality in six U.S. cities. *Journal of Medicine*, 329: 1753-1759.

Eastwood, P. (2008). *Particulate Emissions from Vehicles*. John Wiley and Sons.

Eidels-Dubovoi, S. (2002). Aerosol impacts on visible light extinction in the atmosphere of Mexico City. *The Science of the Total Environment*, 287: 213-220.

Euro 1 standards (EC 93). Directives 91/441/EEC (passenger cars only) or 93/59/EEC (passenger cars and light trucks.

Euro 2 standards (EC 96): Directives 94/12/EC or 96/69/EC.

Euro 3/4 standards (2000/2005): Directive 98/69/EC, further amendments in 2002/80/EC.

Euro 5/6 standards (2009/2014). Regulation 715/2007 (“political” legislation) and several comitology regulations.

European Commission Joint Research Center. (2007) Particle measurement programme (PMP) light-duty inter-laboratory correlation exercise final report. *Institute for Environment and Sustainability*.

Fourth assessment report: Climate change 2007. *Intergovernmental Panel of Climate Change*, Section 2.4.1. http://www.ipcc.ch/publications_and_data/publications_and_data_reports.htm

Franklin, L. (2010). *Effects of homogeneous charge compression ignition (HCCI) control strategies on particulate emissions of ethanol fuel*. PhD. Thesis, University of Minnesota.

Gray, A. W., Ryan, T. W. III. (1997). Homogeneous charge compression ignition (HCCI) of diesel fuel. *SAE Technical Paper Series*, 971676.

Heywood, J. B. (1988). *Internal Combustion Engine Fundamentals*. McGraw-Hill, Inc. p. 601-619.

Hinds, W. C. (1999). *Aerosol Technology — Properties, Behavior, and Measurement of Airborne Particles*. John Wiley and Sons.

Horvath, H. (1993). Atmospheric light absorption-A review. *Atmospheric Environment*, 27A: 293-317.

Horvath, H. (1994). Atmospheric aerosols, atmospheric optics and visibility. *Journal of Aerosol Science*, 25:S23–S24.

Huang, Y., Alger, T., Matthews, R., Ellzey, J. (2001). The effects of fuel volatility and structure on HC emissions from piston wetting in DISI engines. *Society of Automotive Engineers*, 2001-01-1205.

International Commission on Radiological Protection. (1966). Task force of lung dynamics. *Health Physics*, 12:173-207.

Kaiser, E. W., Maricq, M. M., Xu, N., Yang, J. (2005). Detailed hydrocarbon species and particulate emissions from a HCCI engine as a function of air-fuel ratio. *SAE Technical Paper Series*, 2005-01-3749

Kampa, M., Castanas, E. (2008). Human health effects of air pollution. *Environmental pollution*, 151: 362-367.

Karlsson, R. B., Heywood, J. B. (2001). Piston fuel film observations in an optical access GDI engine. *Society of Automotive Engineers*, 2001-01-2022.

Kayes, D., Hochgreb, S. (1999). Mechanisms of particulate matter formation in spark-ignition engines 2: Effect of fuel, oil, and catalyst parameters. *Environmental Science and Technology*, 33:3968-3977.

Kittelson, D. B. (1998). Engines and nanoparticles: A review. *Journal of Aerosol Science*, 29(5/6):575–588.

Kleeman, M. J., Schauer, J. J., Cass, G. R. (2000) Size and composition of fine particulate matter emitted from motor vehicles. *Environmental Science and Technology*, 34: 1132-1142.

Kokhanovsky, A. A. (2008). *Aerosol optics light absorption and scattering by particles in the atmosphere*. Springer-Praxis, Berlin

Li, H., Neill, W., Chippior, W., Graham, L., Connolly, T., and Taylor, J. D. (2007). An Experimental Investigation on the Emission Characteristics of HCCI Engine Operation Using N-Heptane. *SAE Technical Paper Series*, 2007-01-1854.

Lockwood, F. C., van Niekerk, J. E. (1995). Parametric study of a carbon black oil furnace. *Combustion and Flame*, 103: 76-90.

Marshall, J. (2006) Clean-burn engine dodges ever tighter regulations. *New Scientist*, 198:26-27

Mehta, D., Alger, T., Hall, M., Matthews, R., Ng, H. (2001). Particulate characterization of DISI research engine using a nephelometer and in-cylinder visualization. *Society of Automotive Engineers*, 2001-01-1976.

Munro, R. (1990). Emissions impossible – The piston & ring support system. *Society of Automotive Engineers*. 900590

Olfert, J. S. (2006). *On new methods of ultra-fine particle mass classification*. PhD. thesis, University of Cambridge.

Penner, J. E., Hegg, D., and Leaitch, R. (2001). Unraveling the role of aerosols in climate change. *Environmental Science and Technology*, 35:332A–340A.

Pope III, C. A. (2000). Review: Epidemiological basis for particulate air pollution health standards. *Aerosol Science and Technology*, 32:4–14.

Pope III, C. A., Burnett, R. T., Thun, M. J., Calle, E. E., Krewski, D., Thurston, G. D. (2002). Lung cancer, cardiopulmonary mortality, and long-term exposure to fine particulate air pollution. *Journal of the American Medical Association*, 287: 1132-1141.

Pope III, C. A., Thun, M. J., Namboodiri, M. M., Dockery, D. W., Evans, J. S., Speizer, F. E., Heath, Jr. C. W. (1995). Particulate air pollution as a predictor of mortality in a prospective study of U.S. Adults. *American Journal of Respiratory and Critical Care Medicine*, 151: 669-674

Price, P., Stone, R., Misztal, J., Xu, H., Wyszynski, M., Wilson, T., Qiao, J. (2007). Particulate emissions from a gasoline homogeneous charge compression ignition engine. *SAE Technical Paper Series*, 2007-01-0209.

Quader, A. A. (1989). How injector, engine, and fuel variables impact smoke and hydrocarbon emissions with port fuel injection. *Society of Automotive Engineers*, 890623.

Ramanathan, V., Carmichael, G. (2008). Global and regional climate changes due to black carbon. *Nature Geoscience*, 221-227.

Remer, A. L. A., Chin, M., Decola, P., Hq, N., Fein-, G., Kahn, R. A., Quinn, P. K., Rind, D., Giss, N., Schwartz, S. E., Streets, D. G., Yu, H., Umbc, N. G. (2007). Atmospheric aerosol properties and climate impacts. *The U.S. Climate Change Science Program*, Executive Summary.

Schwartz, J., Litonjua, A., Suh, H., Verrier, M., Zanobetti, A., Syring, M., Nearing, B., Verrier, R., Stone, P., MacCallum, G., Speizer, F. E., Gold, D. R. (2005). Traffic related pollution and heart rate variability in a panel of elderly subjects. *Thorax*, 60: 455-461.

Shin, Y., Cheng, W. K. (1997). Engine-out “dry” particulate matter emissions from SI engines. *Society of Automotive Engineers*. 972890.

Stanglmaier, R. H., Ryan, T. W. III, and Souder, J. S. (2001). HCCI Operation of a Dual-Fuel Natural Gas Engine for Improved Fuel Efficiency and Ultra-Low NOx Emissions at Low to Moderate Engine Loads. *SAE Technical Paper Series*, 2001-01-1897.

Taylor, R. (1997). Carbon blacks: Production, properties and applications. *Introduction to Carbon Technologies*: 167-210.

Yang, J., Kenney, T. (2002). Some concepts of DISI engine for high fuel efficiency and low emissions. *Society of Automotive Engineers*, 2002-01-2747.

Zhao, H. (2007). *HCCI and CAI engines for the automotive industry*. Woodhead Publishing.

Chapter 2: Experimental Setup

The experiments are designed to allow for the measurement and analysis of the various properties of PM produced during motoring, SI, and HCCI engine operation. The measurements include the particle size distribution, particle volatility and particle density. In addition, the particle size distribution is measured during transient engine operation.

Two different test engines are used to carry out the tests described in this thesis. The first is a modified cooperative fuel research (CFR) engine used for steady-state experiments. The configuration of this engine is described in detail in section 2.1. The second engine used is a single-cylinder Ricardo engine that has been fitted with electromagnetic valves. This allows for cycle-by-cycle changes in valve timing to test the effects of transient operation on PM emissions. The configuration of this engine is described in section 2.2.

In addition to the combustion engines used, a variety of particulate measurement equipment is used for the different tests. That equipment and the measurement methods are described in section 2.3. The uncertainties associated with these instruments is recorded in Appendix A.

2.1 CFR Engine

A Waukesha CFR engine is used to carry out steady state tests to produce the results described in chapter 3. Some modifications have been made to the engine, as described by Boddez (2011). The engine throttle is located downstream of the intake heater as described in the optimized engine configuration by Boddez. A schematic of the engine identifying the main components is shown in Figure 2.1.

To provide the necessary operating conditions for HCCI combustion, the CFR engine uses compressed air from the building supply, which is regulated to 120 kPa and heated to 140 °C. All tests performed using the CFR engine utilized port injection of compressed natural gas (aside from motoring tests, in which no fuel is injected and the engine is simply being turned over by the dynamometer). The spark plug is only fired during the SI tests, and not during HCCI or motoring. The engine exhaust is sampled immediately downstream of the exhaust valve to measure the particulate emissions, whereas the sampling line for the gas phase emissions is further downstream. The exhaust sample used for particulate emissions testing is conditioned using a two-stage dilution system before flowing to the particulate measurement equipment. The dilution system is discussed in section 2.3.1.

Tests are carried out for motoring and SI operation at low and high compression ratios (10 and 17). HCCI tests are only done with a CR of 17 because it requires a high compression ratio. However, HCCI measurements are made for three different power levels.

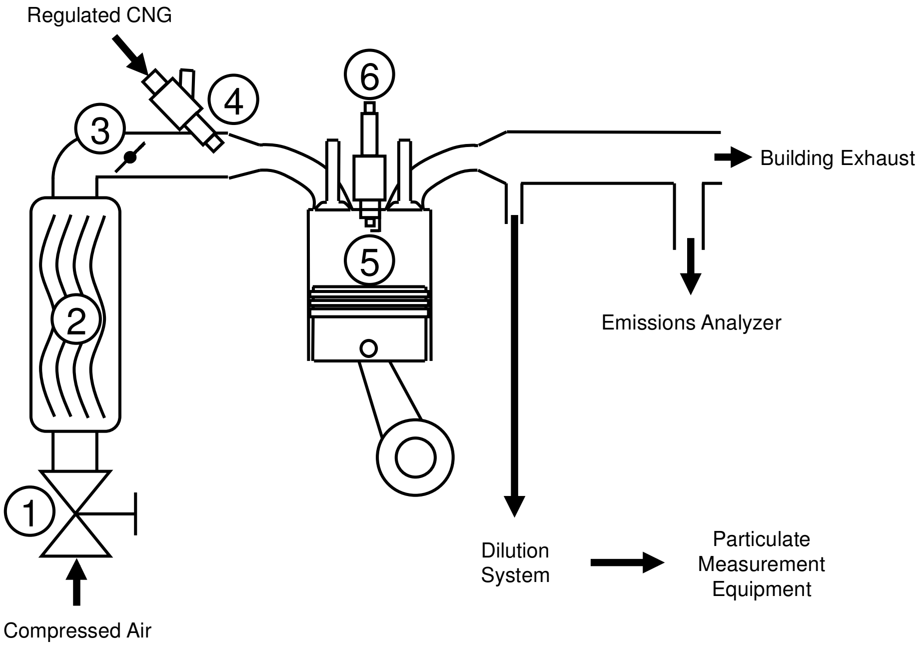

Figure 2.1: CFR Engine setup schematic. Labeled components are (1) air pressure regulator, (2) intake heater, (3) throttle, (4) fuel injector, (5) engine cylinder, and (6) spark plug. Adapted from Handford (2009).

2.2 Ricardo Engine

For transient particulate testing, a single cylinder Ricardo Hydra Mark III engine is used. The engine has been heavily modified and has been fitted with electromagnetic valve controllers. The current configuration of the engine is described in detail by Mashkournia (2008). A schematic of the engine identifying the main components is shown in Figure 2.2.

The engine throttle is upstream of an intake heater, which allows for the necessary conditions to achieve HCCI combustion. The fuel injector is located in the intake port, and the fuel used is iso-octane. The intake and exhaust valve timing is controlled on a cycle-by-cycle basis with the electromagnetic valve controllers. The engine exhaust is sampled immediately downstream of the exhaust valve to measure the particulate emissions using a differential mobility spectrometer (DMS), which is described in more detail in section 2.3.7.

The transient particle emissions are measured when switching between valve timings of 60° and 180° of negative valve overlap (NVO). Negative valve overlap is a measurement of the time when both the intake and exhaust valves are closed during the exhaust and intake strokes.

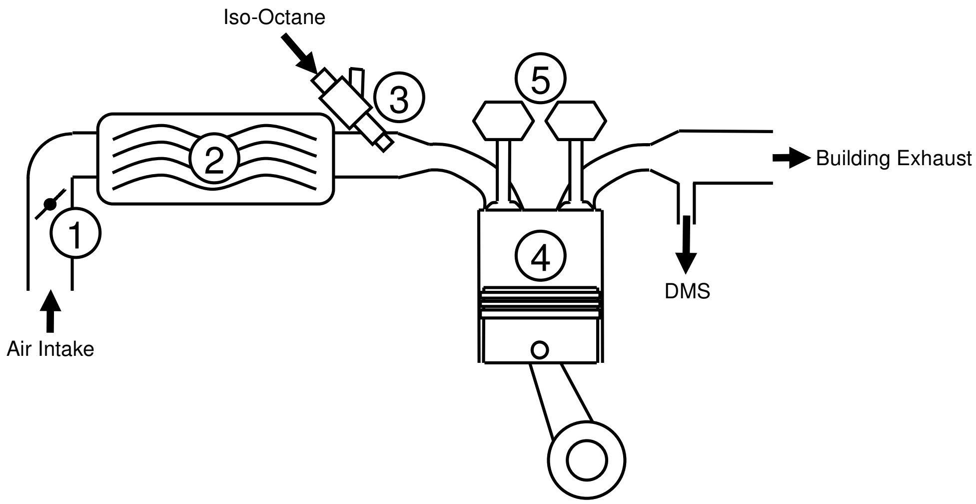

Figure 2.2: Ricardo Engine setup schematic. Labeled components are (1) throttle, (2) intake heater, (3) fuel injector, (4) engine cylinder, and (5) electromagnetic valve controllers. Adapted from Handford (2009).

2.3 Emissions Equipment

2.3.1 Dilution

To measure particulate emissions, the exhaust sample needs to contain particle concentrations within the range of the instruments, as well as avoid condensation of water vapor or other volatile compounds. By diluting the sample, the partial pressure of any vapors is reduced, which eliminates this problem. While the DMS includes a built-in two-stage dilution system, the other emissions equipment requires that the sample be diluted before using the instruments.

The fuel used for the CFR experiments is compressed natural gas. Natural gas is mostly composed of methane, with the balance being made up mainly of ethane, propane, butane, and pentanes. When methane is burned in stoichiometric mixtures it produces two moles of water vapor for every mole of fuel burned as shown in the following equation:

$$\mathrm{CH_4} + 2\,(\mathrm{O_2} + 3.76\ \mathrm{N_2}) \rightarrow \mathrm{CO_2} + 2\mathrm{H_2O} + 7.52\ \mathrm{N_2}$$

The resulting volume fraction of water is 19%. At this concentration, the dew point for water is 60 °C. This means that the exhaust gases must be heavily diluted to avoid condensation of water vapor. To dilute the exhaust gases, they are passed through a two-stage dilution system as shown in Figure 2.3.

The pressurized dilution air is dehumidified using a desiccant dryer to ensure that no moisture is being introduced into the system. Also, to remove any particles present in the dilution air, a HEPA filtration system is used.

The first stage dilution air is heated to 35 °C to avoid rapidly cooling the exhaust sample during mixing. An ejector dilutor is used which is based on that described by Maricq (2003) and is shown below in Figure 2.4. The sample is introduced into a Swagelok tee through a small orifice at atmospheric pressure. The pressurized dilution air is also introduced into the tee. As the dilution air flows through the area between the sample tube and the exit tube, the pressure drops and causes suction on the sample. The diluted sample that exits the dilutor is at ambient pressure. The first stage provided a dilution factor of 10.

After the first stage dilution, a pressure relief line allows for the measurement of unburned hydrocarbon concentration, as well as allowing excess sample to escape from the system and maintain the diluted sample near atmospheric pressure.

The second stage dilution air is kept at ambient temperature and is again mixed using an ejector dilutor and again provides a dilution factor of 10. After the second stage dilution, another pressure relief line allows for the measurement of unburned hydrocarbon concentration, and allows excess sample to escape from the system.

By measuring the unburned hydrocarbon concentration of the undiluted exhaust, as well as the concentrations after the first and second stages of dilution, a dilution factor of 10 is measured for each stage, providing a total exhaust sample dilution of 100. After dilution, the concentration of water is 0.19%, meaning that the dewpoint would be near 0 °C.

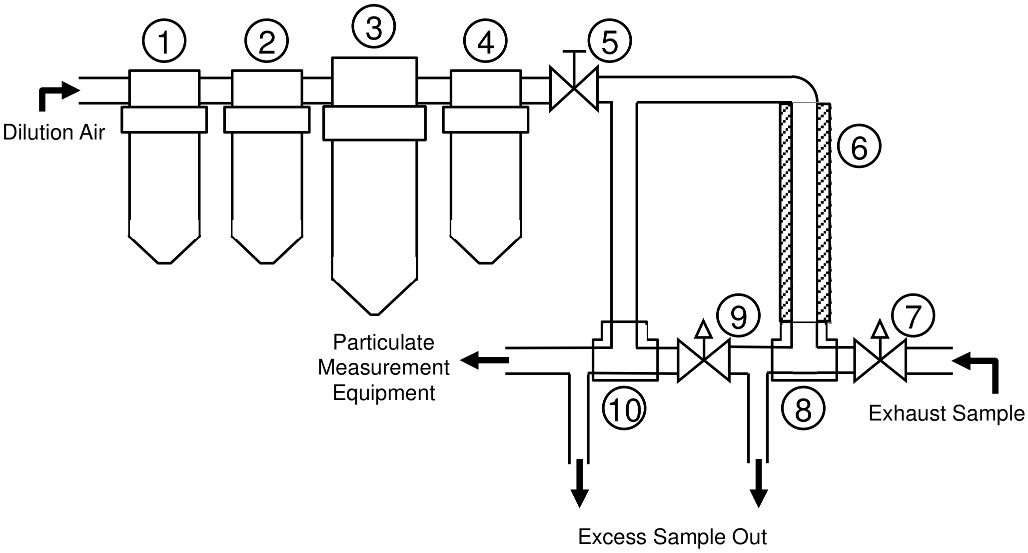

Figure 2.3: Schematic of two-stage dilution system. Labeled components are (1) grade 10 particulate filter (2) grade 6 particulate filter, (3) desiccant dryer, (4) absorber, (5) pressure regulator, (6) line heater, (7) needle valve, (8) ejector dilutor, (9) needle valve, and (10) ejector dilutor. Adapted from Handford (2009).

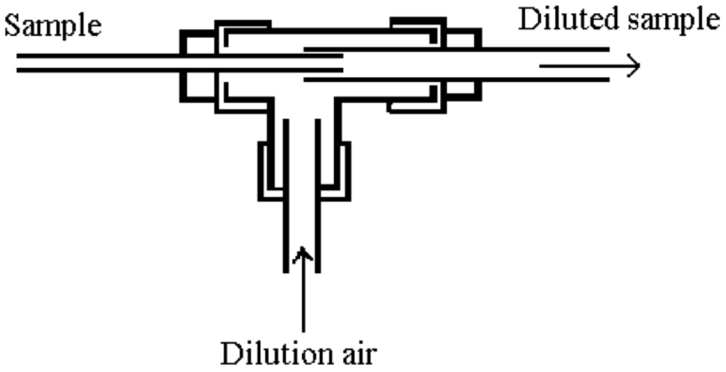

Figure 2.4: Schematic of ejector dilutor used in both stages. Figure from Ghazi (2012).

2.3.2 Thermodenuder

A Thermodenuder is used to evaporate volatile material that has nucleated or has condensed on non-volatile particles. The thermodenuder is made from a long section of ¼" copper tubing which allows the sample to be heated to a controlled temperature and then allows the sample to cool. The first section of the thermodenuder is 63 cm long. A heating tape is wrapped around the tubing and covered in insulation. A thermocouple attached to the outside wall of the copper tubing at the end of the heated section allows the temperature to be controlled. The cooling section is 110 cm long and is not insulated allowing the heat to dissipate. The effectiveness of the thermodenuder in vaporizing volatile material was tested by Ghazi (2013).

2.3.3 DMA

The differential mobility analyzer (DMA) is an instrument, developed by Knutson (1975), that is used to classify particles based on their electrical mobility equivalent diameter. Otherwise known as the mobility diameter, d_m is the diameter of a sphere with the same velocity in an electrostatic field as the sample particle. The DMA samples the exhaust gases, charges the particles using a bipolar charger, and then introduces the sample into the outside of cylindrical chamber with a central rod that is set to a chosen voltage. In addition to the aerosol flow, a laminar sheath flow is introduced into the chamber, causing the aerosol to flow in the axial direction. The rod is given a negative voltage and creates a uniform electrical field. The positively charged particles are attracted to the negatively charged rod in the center, which causes the particles to move in an inward radial direction. The electrostatic force is opposed by the drag force, which resists the particle movement. The radial velocity depends on the charge of the particle as well as the diameter. The force due to the electrical field is represented by:

$$F_{\mathrm{e}} = neE$$

where n is the number of charges on the particle, e is the unit charge, and E is the strength of the electrical field. The drag force is represented by:

$$F_{\mathrm{d}} = \frac{3\pi\mu V d_{\mathrm{p}}}{C_{\mathrm{c}}(d_{\mathrm{p}})}$$

where μ is the viscosity of gas, V is the velocity of the particle, d_{p} is the diameter of the particle, and C_{c} is the slip correction factor, which is a function of d_{p}. For aerosol particle measurements, the assumption can be made that the relaxation time is negligible, causing the particle to reach its terminal velocity almost instantly. Because of this, the electrical and drag forces are equal and the velocity of the particle is:

$$V = \frac{neEC_{\mathrm{c}}(d_{\mathrm{p}})}{3\pi\mu d_{\mathrm{p}}}$$

Therefore, as the particles flow in the axial direction, they are attracted toward the center of the chamber due to the electrical field. Particles with a smaller diameter have greater mobility and therefore move toward the center more quickly, and particles with a greater diameter move toward the center more slowly. Based on the selected voltage, particles of a corresponding size reach the central rod at the correct location to be able to exit through a slot that allows them to pass through the DMA as a monodisperse aerosol. A schematic of the DMA is shown in Figure 2.5.

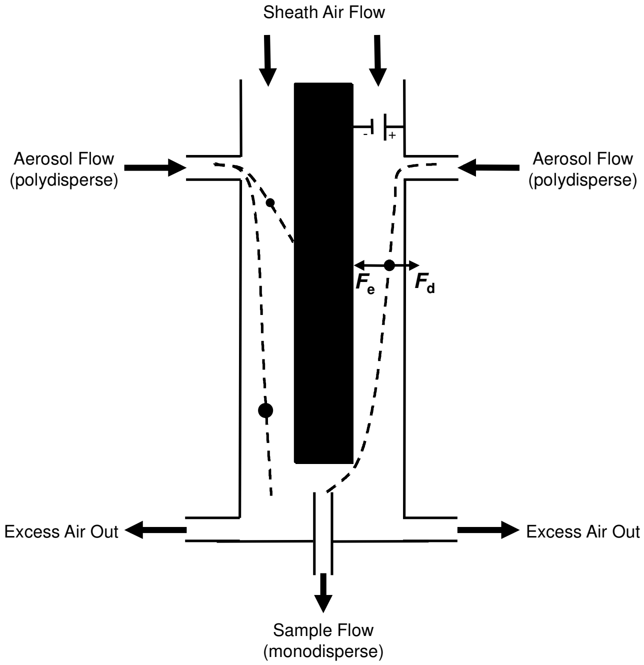

Figure 2.5: Schematic of DMA.

2.3.4 CPC

The condensation particle counter (CPC) was developed by Agarwal (1978). It is an optical particle counter that can detect particles as small as 2.5 nm. An aerosol is passed into the CPC, which is mixed with a sheath flow saturated with butanol vapor. The mixture is then passed through a condenser, which causes the butanol to condense on the particles, increasing their size and allowing them to be detected by the optical counter. The CPC is then able to determine the particle concentration.

2.3.5 SMPS

When a DMA is used in series with a CPC it is referred to as a scanning mobility particle spectrometer (SMPS). By scanning the voltage of the DMA and measuring the concentration of particles for each voltage, a particle size distribution can be constructed.

Because of the time that it takes to scan the voltage and make concentration measurements at each voltage, using an SMPS requires a steady-state aerosol flow.

2.3.6 CPMA

The centrifugal particle mass analyzer (CPMA) was developed by Olfert et al (2005) and consists of two concentric cylinders that rotate at different speeds generating a velocity profile, which results in a radially-decreasing centrifugal force in the space between the two cylinders. A high voltage controller charges the inner cylinder, which attracts negatively charged particles. The electrostatic force is opposed by the centrifugal force. For a given rotational speed, and a given voltage, only particles of a certain mass-to-charge ratio will pass through the instrument without impacting on either cylinder. The CPMA was developed as an improvement to the aerosol particle mass analyzer (APM), in which both cylinders rotate at the same rotational speed, resulting in a lower transfer efficiency (Ehara, 1996).

The CPMA is also often connected to a CPC, and by scanning the voltage of the inner cylinder and/or the cylinders' rotational speed, the mass distribution of an aerosol can be constructed. Also, the particles' mobility diameter is known, the density of the particles can then be determined. A schematic of the CPMA can be seen in Figure 2.6.

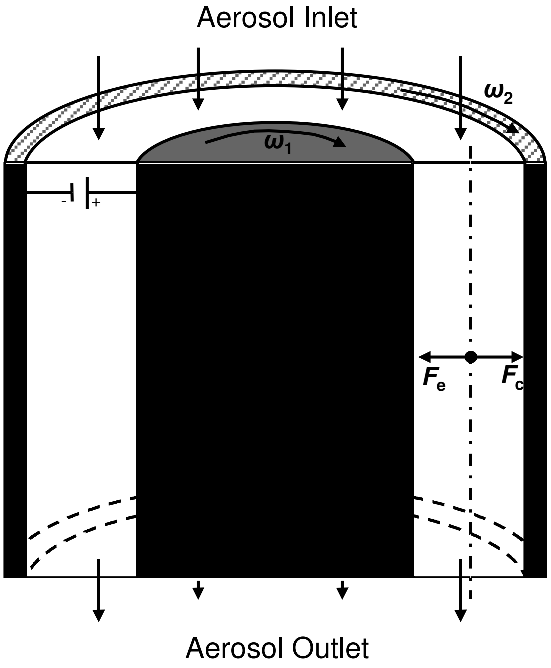

Figure 2.6: Schematic of CPMA.

2.3.7 DMS

The differential mobility spectrometer (DMS) operates on a similar principle to the DMA, and again classifies particles based on their mobility diameter, d_m. The DMS was developed by Reavell (2002). The aerosol particles are charged using a unipolar corona charger and are then introduced at the inside of a cylindrical chamber with a central high voltage electrode along with a sheath flow, causing the particles to move in the axial direction. Both the particles and the electrode have a positive charge, causing the particles to move toward the outside of the cylindrical chamber. This force is once again balanced by the drag force. The outside of the cylindrical chamber consists of a series of electrometer rings, which detect the impaction of any charged particles. Smaller particles have a greater radial velocity, causing them to impact upon the earlier rings, whereas larger particles have a lower radial velocity causing them to impact upon the later rings. By measuring the voltage on each ring, the particle size distribution is constructed. Also, because of a fast time response (10-90% rise time of 500 ms), the DMS is useful in measuring transient particle distributions.

The DMS uses a two-stage dilution system and heated line to condition the sample that is being tested. The sampling head is attached directly to the engine exhaust manifold immediately downstream of the exhaust valve and contains a cyclone diluter, which allows for large particles (~10 μm) to be eliminated from the sample as the DMS cannot measure that size of particles. After the first dilution stage, the DMS uses a heated sampling line to ensure that the exhaust sample does not cool and cause volatile material to condensate. Once the sample reaches the DMS, it is diluted again (using a disc dilutor) before the particles are charged and passed through the classifier. A schematic of the DMS and the sampling head can be seen in Figure 2.7.

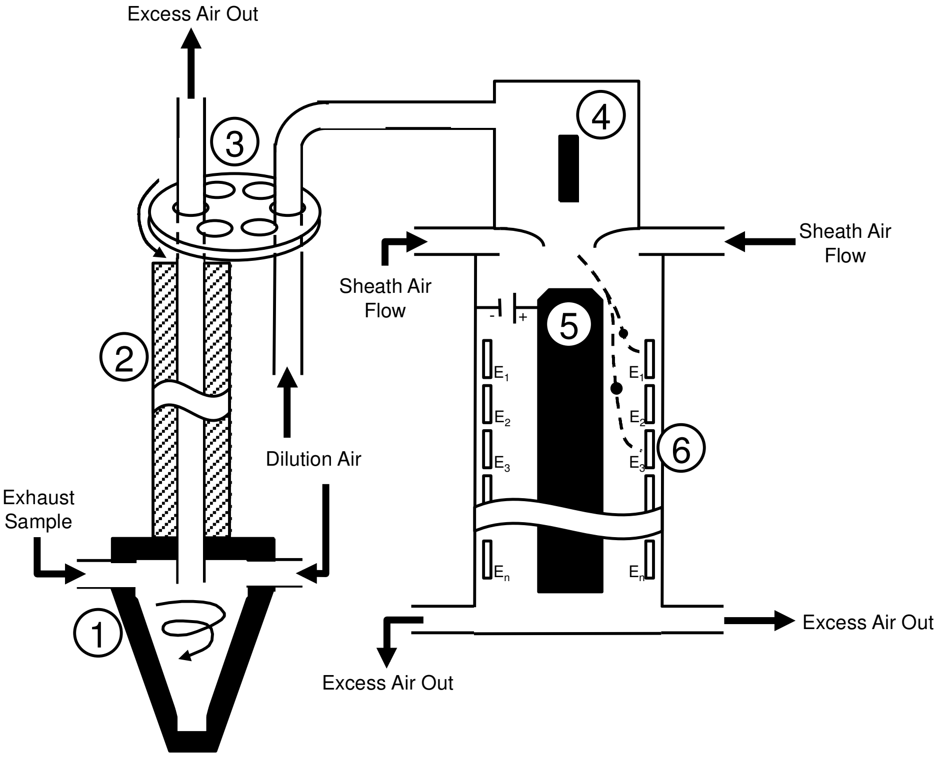

Figure 2.7: Schematic of DMS. Labeled components are (1) sampling head with cyclone dilutor, (2) heated sample line, (3) disc dilutor, (4) corona charger, (5) high voltage electrode, and (6) electrometer rings.

2.4 References

Agarwal, J. K., Sem, G. J., 1978. Generating submicron monodisperse aerosol for instrument calibration. *TSI Quarterly*, 3-8.

Boddez, J. (2011). *Evaluation of SI-HCCI-SI Mode-Switching Using Conventional Actuation on a CNG Engine*. Master's thesis, University of Alberta.

Ehara, K., Hagwood, C., Coakley, K. J., 1996. Novel method to classify aerosol particles according to their mass-to-charge ratio-aerosol particle mass analyser. *Journal of Aerosol Science*, 27: 217-234.

Ghazi, R., Olfert, J. S. (2013). Coating mass dependence of soot aggregate restructuring due to coatings of oleic acid and dioctyl sebacate. *Aerosol Science and Technology*, 47:192-200.

Handford, D. I. (2009). *Direct Injection Assisted HCCI Combustion of Natural Gas*. Master's thesis, University of Alberta.

Knutson, E. O., Whitby, K. T., 1975. Aerosol classification by electric mobility: apparatus, theory, and applications. *Journal of Aerosol Science*, 6: 443-451.

Maricq, M. M., Harris, S.J., Szente, J. J., (2003). Soot size distributions in rich premixed ethylene flames. *Combustion and Flame*, 132: 328 -342.

Mashkournia, M. (2012). *Electromagnetic Variable Valve Timing on a Single Cylinder Engine in HCCI and SI*. Master's thesis, University of Alberta.

Olfert, J. S., Collings, N., 2005. New method for particle mass classification - the Couette centrifugal particle mass analyzer. *Journal of Aerosol Science*, 36: 1338-1352.

Reavel, K., Hands, T., Collings, N. (2002). A Fast Response Particulate Spectrometer for Combustion Aerosols. *SAE Technical Paper*, 2002-01-2714.

Chapter 3: Steady-State Particulate Measurements

Upcoming automotive particulate emission regulations include both a measurement of the number of non-volatile particulates, and the mass concentration of the total PM. Because of this, it is increasingly important to understand the physical properties of PM emissions from combustion. Also, an investigation of the effects of different parameters allows for increased understanding of the formation mechanism for these particles, which will allow for the development of strategies to further reduce engine emissions.

3.1 Testing Methodology

A CFR engine with variable compression ratio, as described in detail in Chapter 2, is used during motoring, SI, and HCCI operation modes to measure the steady-state particulate emission distributions, as well as determine the volatility and density of the measured PM. All tests performed by sampling the CFR engine exhaust are diluted using a two-stage diluter with an overall dilution factor of 100. The configuration of the particulate measurement equipment for each of these tests can be seen in Figure 3.1

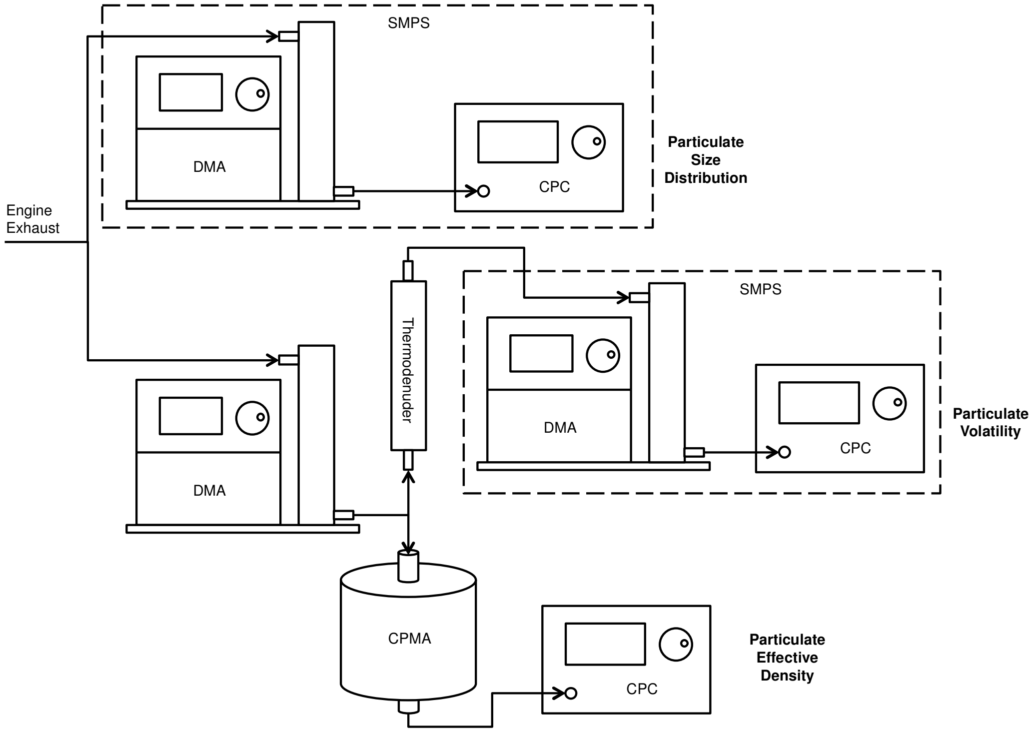

Figure 3.1: Aerosol classification equipment used to measure the particle size distribution, particulate volatility, and particulate effective density.

3.1.1 Size Distributions

The size distributions are measured using a DMA (Knutson, 1975) and CPC (Agarwal, 1978) in series, creating an SMPS. The particles measured consist of both solid and volatile compounds. These measurements are obtained during motoring and SI operation with compression ratios of 10 and 17. The compression ratio of 10 reflects more typical conditions of a SI engine, whereas the compression ratio of 17 is more typical for HCCI combustion. This higher compression ratio is necessary to achieve the needed operating conditions for HCCI on this engine. The particle size distributions are also measured during HCCI operation with a compression ratio of 17 for three different power levels.

3.1.2 Particulate Volatility

By removing volatile material, it is possible to effectively measure the non-volatile particle number, which will soon be a regulated value. To study the volatility of the exhaust PM, the exhaust samples are heated to increasing temperatures before the resulting particle size and number is measured. This test is done during motoring and SI operation with compression ratios of 10 and 17, as well as during HCCI operation with a compression ratio of 17 for three different power levels. First, a DMA is used to select particles with the same size as the geometric mean diameter (GMD) of the polydisperse distribution as measured with the SMPS. Those particles are then passed through a thermodenuder (Ghazi, 2013), heated to temperatures of 30, 50, 100, and 150 °C. Afterward, the size distribution of the remaining particles is measured using an SMPS in a similar manner to that used by Sakurai et al (2003) and Surawski et al (2010). This allows observation of the change in the median particle diameter and the change in total particle number.

3.1.3 Particulate Effective Density

The PM effective density during the different operating modes is also measured. This is done by sampling the exhaust during motoring, SI, and HCCI with compression ratios of 17. The DMA is used to select particles of a certain size (monodisperse). The selected particles are then passed into the CPMA (Olfert et al, 2005) as the voltage is scanned. For each voltage, particles of a specific mass are able to pass through the instrument. Finally, a CPC is used to detect the particles that successfully pass through the CPMA. Given that the particles are of a known mobility-equivalent diameter, the measured mass of the particles can be used to calculate the effective density for particles of the selected size, where the effective density is defined as the mass of the particle divided by the volume of the mobility-equivalent sphere. For spherical particles (with no internal voids) the effective density is equal to the material density of the particulate matter. The density is measured for particles of 30 to 150 nm.

3.2 Experimental Results

3.2.1 Particulate Matter Size Distributions

The operating conditions and PM data collected using the SMPS is summarized in Table 3-1. Data collected while motoring at compression ratios of 10 and 17 are compared in Figure 3.2. For a compression ratio of 10, the GMD is 31.2 ± 0.9 nm and the geometric standard deviation (GSD) of the particle distribution is 1.53. The average particle concentration is $1.8\text{x}10^8 \pm 1.8\text{x}10^7$ cm^{-3} (all uncertainties are given with 95% confidence). For a compression ratio of 17, the particle size distribution has a GMD is 65.9 ± 2.0 nm with a GSD of 1.54. The average particle concentration is $3.3\text{x}10^8 \pm 3.3\text{x}10^7$ cm^{-3}. Franklin (2010) had significantly smaller particles with a GMD of around 21 nm at high compression ratio.

The SMPS data collected while operating in SI mode at compression ratios of 10 and 17 are compared in Figure 3.3. For a compression ratio of 10, the GMD is 27.9 ± 1.1 nm with a GSD of 1.64. The average particle concentration is $1.0\text{x}10^8 \pm 1.0\text{x}10^7$ cm^{-3}. For a compression ratio of 17, the GMD is 42.1 ± 1.5 nm with a GSD of 1.50. The average particle concentration is $2.4\text{x}10^8 \pm 2.4\text{x}10^7$ cm^{-3}. In the case of both motoring and SI operation, this shows that a higher compression ratio results in a larger GMD as well as a greater particle concentration. Also, it is important to note that, while the size distribution for SI at a compression ratio of 10 was slightly bimodal, which could suggest an accumulation mode of non-volatile PM, both modes were made of volatile material, as shown below in section 3.2.2.

During HCCI mode, the SMPS was used to collect data for three different power levels, all at a compression ratio of 17, which are compared in Figure 3.4. The three power levels are 3.5 bar, 4.0 bar, and 4.7 bar indicated mean effective pressure (IMEP) with an engine speed of 700 rpm. The GMDs are 48.0 ± 1.6 nm, 41.0 ± 1.3 nm, and 37.0 ± 1.2 nm with GSDs of 1.51, 1.47, and 1.47, respectively. The average particle concentrations are $2.6\text{x}10^{8} \pm 2.6\text{x}10^{7}$ cm^{-3}, $2.7\text{x}10^{8} \pm 2.7\text{x}10^{7}$ cm^{-3}, and $2.2\text{x}10^{8} \pm 2.2\text{x}10^{7}$ cm^{-3}. Franklin (2010) showed slightly smaller particle distributions with GMDs for different loads ranging from approximately 20 to 35 nm.

The key values for all operating conditions, including total particle number and total particle mass (volatile and non-volatile), are summarized in Table 3.1. As is shown, a significant particulate mass is shown during all operating conditions, including motoring. This suggests that the PM contains material that is not a result of combustion products or incomplete combustion, such as soot. The most likely source is engine oil. During all operating conditions, including motoring, the cylinder and the engine oil on the cylinder wall gets hot. This can result in semi-volatile material evaporating from the engine oil, which later condenses to form the particulate matter.

Franklin (2010) measured the particle distributions during motoring and ethanol HCCI engine operation in a similar manner. While Franklin measured particle concentrations of the same magnitude, the GMD of the measured particles was significantly smaller. For instance, during motoring at a high compression ratio, Franklin had a maximum normalized concentration of $5.8\text{x}10^{8}$ cm^{-3} at approximately 20 nm. This compares to a maximum normalized concentration of $7\text{x}10^{8}$ cm^{-3} at 65.9 nm in this study. This difference suggests that the overall particle mass is greater by nearly two orders of magnitude. This is likely due to the difference in engine. Franklin is using an Isuzu 4HK-1TC, whereas the CFR engine is an older engine and is likely to have higher oil consumption.

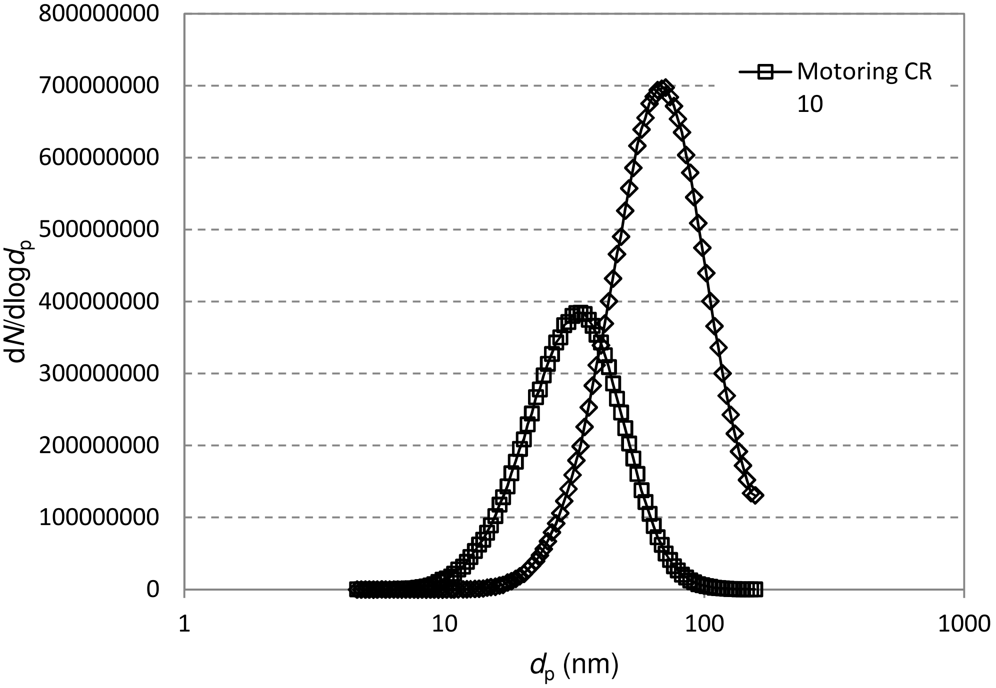

Figure 3.2: Comparison of particle size distributions during motoring at low and high compression ratios.

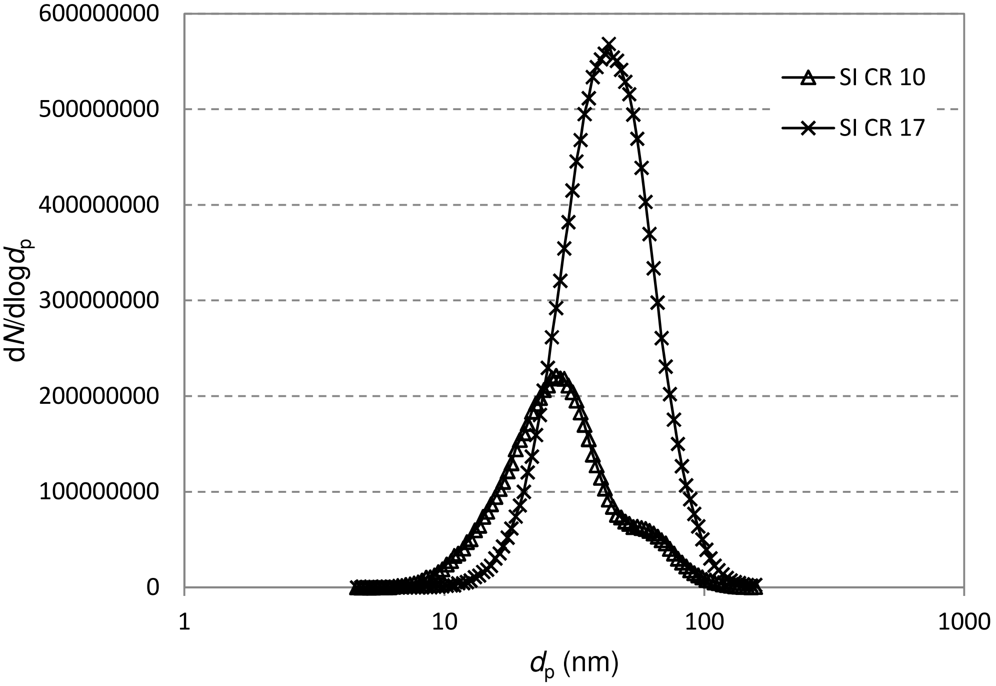

Figure 3.3: Comparison of particle size distributions during SI at low and high compression ratios.

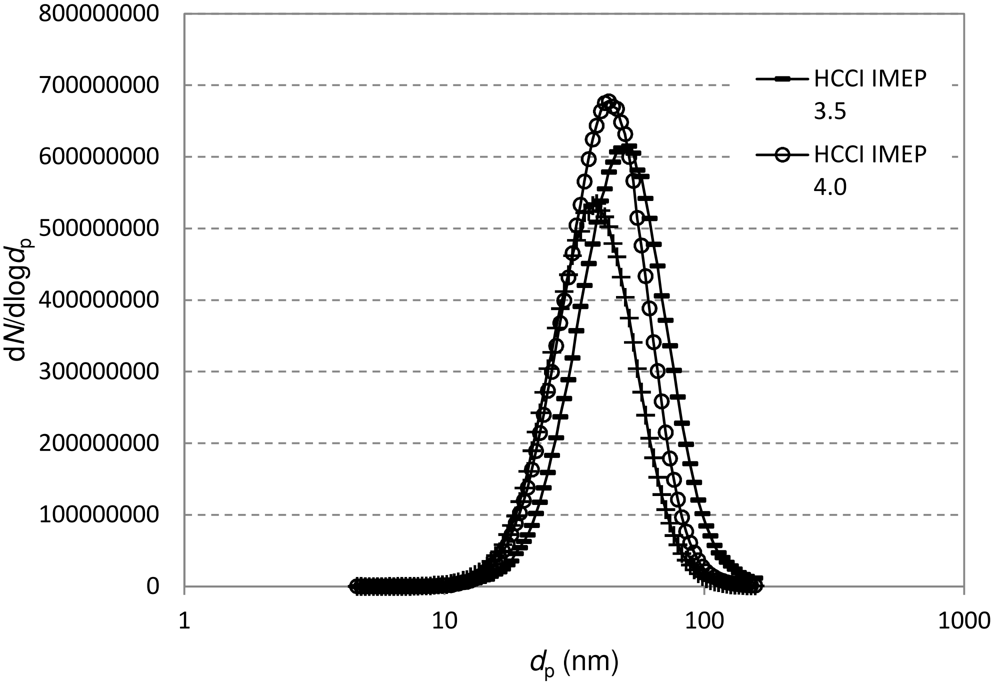

Figure 3.4: Comparison of particle size distributions during HCCI at three different power levels.

Table 3-1: Engine and PM parameters for all operating conditions. Particulate number (N) and mass (M) include both volatile and non-volatile particles. Particle density is assumed to be 850 kg/m^3, based on section 3.2.3.

Mode	CR	IMEP (bar)	Φ	GMD (nm)	GSD	N (cm^{-3})	M (g/cm^3)
Motoring	10	-	-	31.2	1.53	1.8E+8	5.4E-9
Motoring	17	-	-	65.9	1.54	3.3E+8	9.7E-8
SI	10	2.5	0.99	27.9	1.64	1.0E+8	3.0E-9
SI	17	2.8	1.01	42.1	1.50	2.4E+8	1.7E-8
HCCI	17	3.5	0.31	48.0	1.51	2.6E+8	2.8E-8
HCCI	17	4.0	0.42	41.0	1.47	2.7E+8	1.6E-8
HCCI	17	4.7	0.51	37.0	1.47	2.2E+8	9.6E-9

3.2.1.1 Compression Ratio Effects

For both motoring and SI operation, a significant increase in particle concentration is observed when moving from low to high compression ratio. For HCCI combustion, a higher compression ratio is required, so the comparison between low and high compression ratio could not be made. However, Figure 3.5 shows that for all three HCCI operating conditions, the total volume is higher than the low compression ratio tests, and is of a similar magnitude to the other high compression ratio tests. It is also evident that a higher compression ratio results in a larger GMD for the particles present. With both a higher concentration, and a larger GMD, a higher compression ratio results in a greater overall mass of PM.

Increased cylinder pressure causes higher temperatures during compression. Also, the pressure in the cylinder during compression causes air to be forced past the compression rings, otherwise known as blow-by. As the pressure in the cylinder decreases, that air moves back into the cylinder, bringing engine oil with it. Higher pressure in the cylinder results in more blow-by, and therefore more oil being forced into the cylinder. The availability of more engine oil, as well as the increased cylinder temperatures, results in more semi-volatile material evaporating, which then leads to more gas to particle conversion.

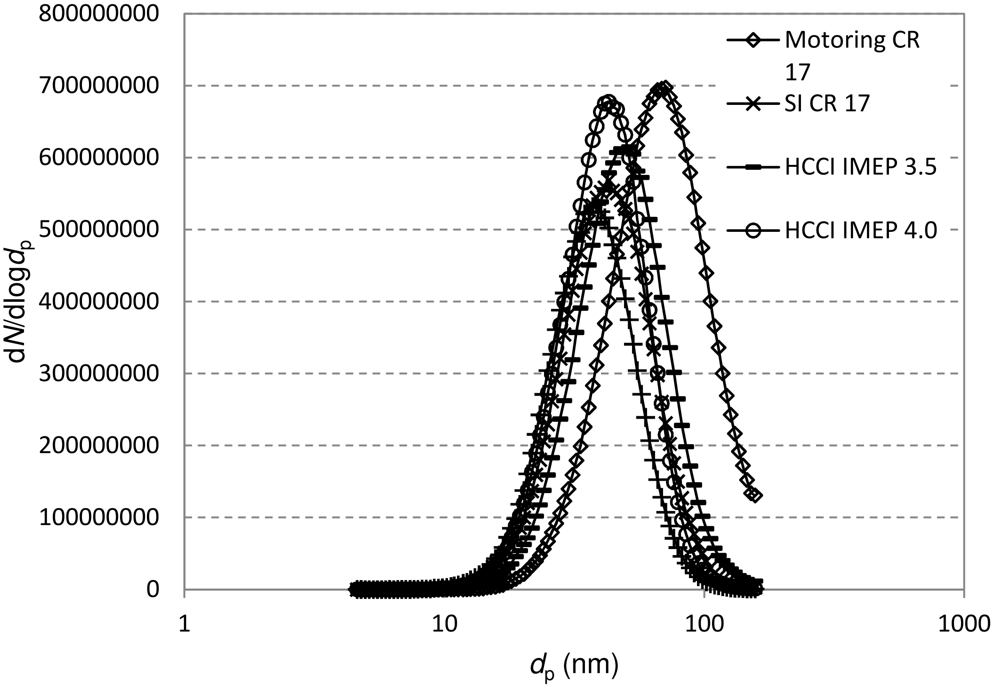

Figure 3.5: Comparison of particle size distributions during motoring, SI, and HCCI (three different power levels) at high CR.

3.2.1.2 Power Level Effects

By comparing the particle distributions from Figure 3.4 of three different power levels during HCCI combustion, it can be noted that increased power production results in decreased GMD. And while the average particle concentration does not follow any particular trend, the total mass decreases with increasing power level. The PM total masses are 2.8x10^{-8} g/cm^3 for 3.5 bar, 1.6x10^{-8} g/cm^3 for 4.0 bar, and 9.6x10^{-9} g/cm^3 for 4.7 bar.

3.2.1.3 Operating Mode Effects

Based on a comparison of the tests performed at the same compression ratio, the highest particulate concentration and the largest GMD are seen during motoring. This remains true for both compression ratios, as seen in Figures 3.5 and 3.6. When operating in SI or HCCI mode, the GMD and particle concentration decrease in comparison to motoring data for the same compression ratio. This suggests that hydrocarbons from the engine oil (that would otherwise contribute to the PM) are combusted. Also, while heavier fuels such as diesel would have a tendency to condense in the exhaust contributing to the PM present, this is not case with natural gas which was used in these tests.

The comparison of particle size and concentration between SI and HCCI operation show very similar PM production, as shown in Figure 3.5.

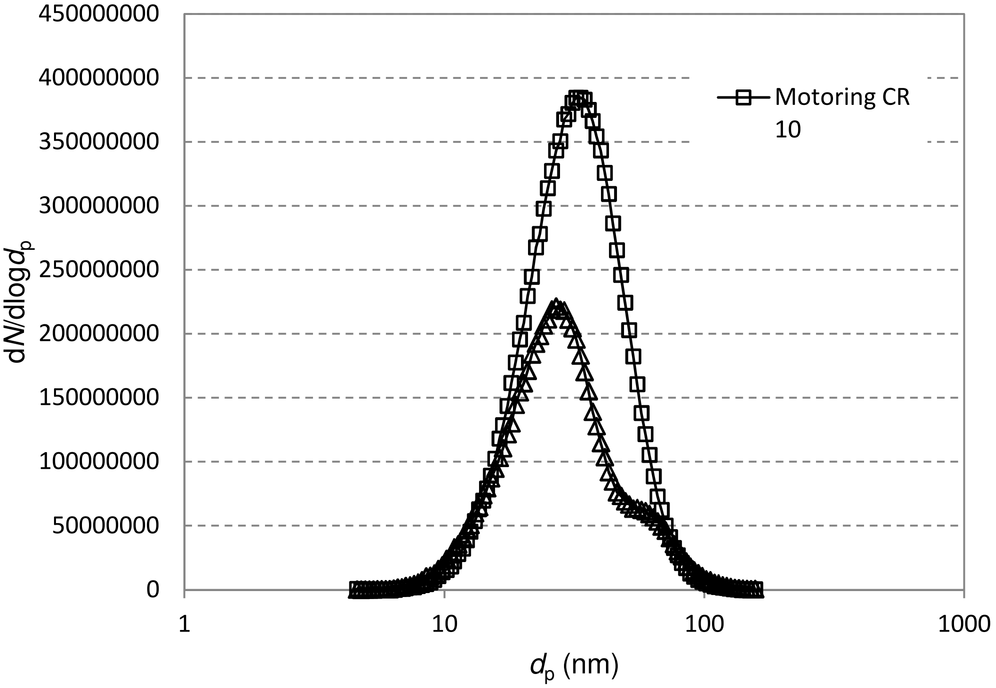

Figure 3.6: Comparison of particle size distributions during motoring and SI at low CR.

3.2.2 Non-volatile Particulate Matter

As a means of determining the amount of PM that is non-volatile, the remaining volume fraction is calculated after DMA-selected particles were denuded using increasing temperature. The total particulate volume remaining is expressed as a fraction of the amount obtained when the denuder was heated to 30 °C, and the volume fraction is measured with denuder temperatures of 50, 100, and in some cases, temperatures as high as 250 °C. The results are shown in Figure 3.7.

The denuder tests show that for all operating conditions the remaining volume fraction is less than 5% after denuding the sample at 100 °C. This applies to motoring, SI, and HCCI operating conditions. For some operating conditions, the sample is denuded at even higher temperatures. It can be seen that the remaining volume fraction for all HCCI power levels is less than 1% at 150 °C. Also, for motoring at a high compression ratio, by denuding the sample at 250 °C, the remaining volume fraction is approximately 0.05%.

Franklin (2010) previously tested ethanol HCCI emissions to investigate the remaining volume fraction of PM after thermal conditioning. Franklin's results also demonstrated that the majority of the particulate matter was removed below 100 °C. He showed that nearly 98% of PM was volatile during HCCI operating conditions for all fired engine loads. However, he also showed that only 80% of PM produced during motoring was volatile. This data is also shown in Figure 3.7.

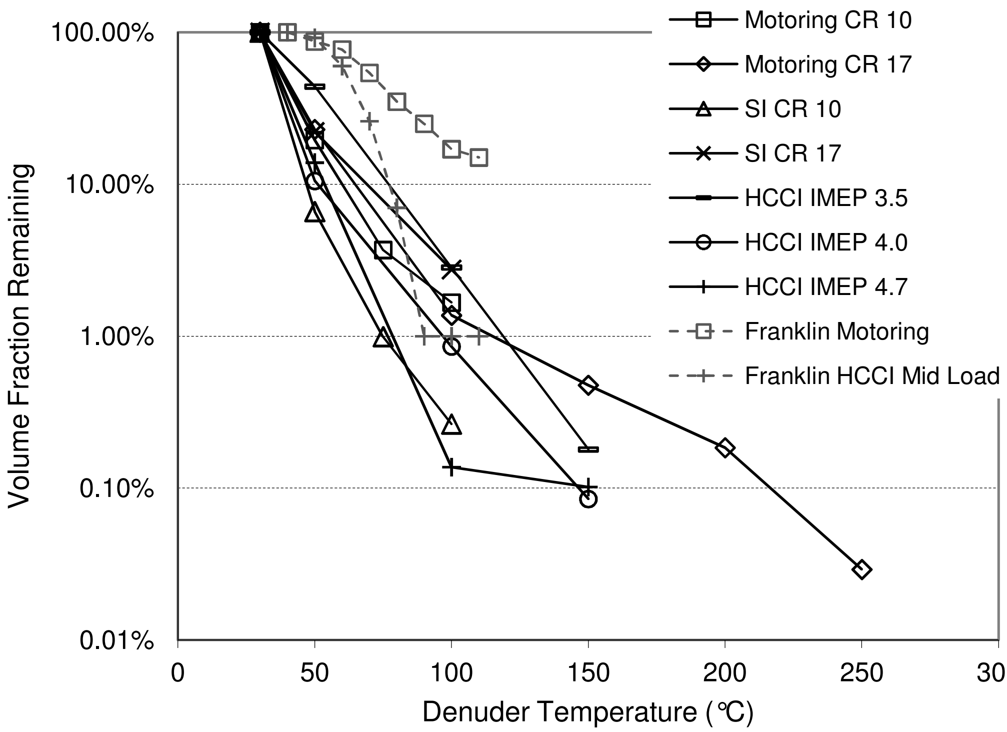

Figure 3.7: Volume fraction remaining after denuding. Measured for motoring and SI at low and high CR, and for three HCCI loads. Also showing remaining volume fraction of PM in ethanol HCCI exhaust after thermal conditioning from Franklin (2010). Shown on a log scale.

Results similar to Franklin (2010) were obtained by heating the exhaust samples during different HCCI loads, however, the results during motoring showed a very similar volume fraction remaining as for HCCI, whereas Franklin showed a much higher volume fraction remaining during motoring.

Franklin suggests in his experiments that PM produced during HCCI was primarily formed from engine oil. Tobias et. al. (2001), using thermal desorption particle beam mass spectrometry, found the volatile component of diesel PM was mainly composed of engine oil. Sakurai (2003) performed mass spectrometry on diesel particulate matter and was able to determine that the PM was mainly composed of *n*-alkanes of C24 to C32, which are similar to components of engine oil. By heating *n*-alkanes of C24 to C32 in a thermodenuder similar to the one used in this study, Sakurai obtained similar evaporation profiles, which showed that nearly all of the PM was removed below a temperature of 100 °C. Due to the volatility of the PM present in the current tests, it can be concluded that the engine oil similarly contributes here, especially since the natural gas would not directly condense and form particulate matter.

3.2.3 Particulate Matter Effective Density

Using the selected diameter from the DMA and the resulting particle masses from the CPMA, the effective densities of particles ranging from 30 nm to 150 nm during motoring, SI, and HCCI are shown in Figure 3.8. For the sake of comparison, the effective density of soot particles from a Diesel engine as measured by Olfert et al (2007) is included. The density measurements have an uncertainty of ± 12% due to error when using a DMA and CPC as determined by Johnson (2013).

The results show a relatively constant effective density for all operating modes. This suggests that the particles are spherical, and presumably made of a liquid, supporting the evidence that the particles are primarily engine oil.

With the exception of a few outliers at low mobility-equivalent diameters (poor counting statistics at these sizes may have contributed to them being outliners), the rest of the values are of a constant density within error of approximately 850 kg/m^3. This is a reasonable value for the density of engine oil.

Because the CPMA relies on the mobility-equivalent diameter, a large non-spherical particle will have an effective density lower than the material density of the particle. While soot has a material density of approximately 1800 kg/m^3 (Park et al, 2004), it has a much lower effective density because of the fractal, non-spherical, morphology of the particle. The difference between effective and material density becomes more pronounced with increasing particle size as is seen in Figure 3.8.

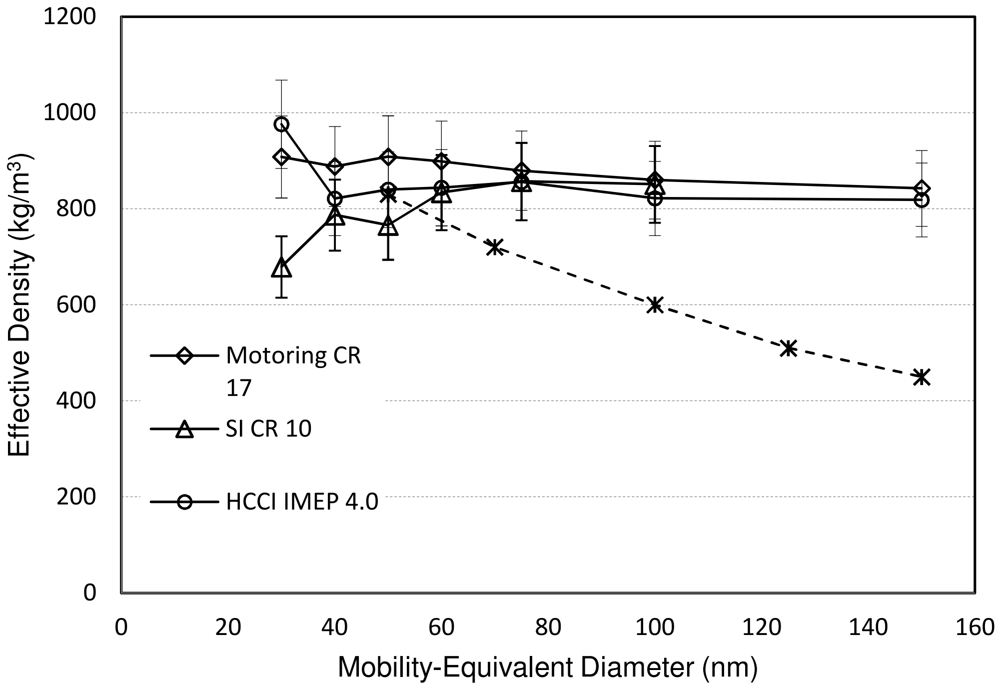

Figure 3.8: Comparison of particle density for different operating modes with 9.4% uncertainty including sample data for effective density of diesel soot per Olfert (2007).

3.3 Conclusions

By measuring the particle size distribution during motoring, SI, and HCCI operation, it can be seen that during SI and HCCI operation, both the size and concentration of PM present are reduced, suggesting that some of the volatile material that would otherwise contribute to the PM is combusted.

It is also shown that for all operating conditions, less than 5% of the PM remains after denuding the exhaust at a temperature of 100 °C, and that even less material remains when treated at a higher temperature. This allows the conclusion to be drawn that the PM is almost completely volatile.

The effective density of the PM during motoring, SI, and HCCI also shows a fairly constant effective density over the range of particle sizes, and that the density is reasonable for that of engine oil.

3.4 References

Agarwal, J. K., Sem, G.J., 1978. Generating submicron monodisperse aerosol for instrument calibration. *TSI Quarterly*, 3-8.

Franklin, L. (2010). *Effects of homogeneous charge compression ignition (HCCI) control strategies on particulate emissions of ethanol fuel*. PhD. Thesis, University of Minnesota.

Ghazi, R., Olfert, J. S. (2013). Coating mass dependence of soot aggregate restructuring due to coatings of oleic acid and dioctyl sebacate. *Aerosol Science and Technology*, 47:192-200.

Johnson, T. J., Symonds, J. P. R., Olfert, J. S. (2013). Mass-mobility measurement using a centrifugal particle mass analyzer and differential mobility spectrometer. *Aerosol Science and Technology*, 10.1080/02786826.2013.830692.

Knutson, E. O., Whitby, K.T., 1975. Aerosol classification by electric mobility: apparatus, theory, and applications. *Journal of Aerosol Science*, 6: 443-451.

Olfert, J. S., Collings, N., 2005. New method for particle mass classification - the Couette centrifugal particle mass analyzer. *Journal of Aerosol Science*, 36: 1338-1352.

Olfert, J. S., Symonds, J. P. R., Collings, N. (2007). The effective density and fractal dimension of particles emitted from a light-duty diesel vehicle with a diesel oxidation catalyst. *Journal of Aerosol Science*, 38:69-82.

Park, K., Kittelson, D. B., Zachariah, M. R., and McMurry, P. H. (2004). Measurement of Inherent Material Density of Nanoparticle Agglomerates. *J. Nanopart. Res.*, 6:267–272.

Sakurai, H., Tobias, H. J., Park, K., Zarling, D., Docherty, K. S., Kittelson, D. B., McMurry, P. H., Ziemann, P. J. (2003). On-line measurements of diesel nanoparticle composition and volatility. *Atmospheric Environment*, 37: 1199-1210.

Surawski, N. C., Miljevic, B., Roberts, B. A., Modini, R. L., Situ, R., Brown, R. J., Bottle, S. E., Ristovski, Z. D. (2010). Particle emissions, volatility, and toxicity from an ethanol fumigated compression ignition engine. *Environmental Science and Technology*, 44: 229-235.

Tobias, H. J., Beving, D. E., Ziemann, P .J., Sakurai, H., Zuk, M., McMurry, P. H., Zarling, D., Waytulonis, R., Kittelson, D .B. (2001). Chemical analysis of diesel engine nanoparticles using a Nano-DMA/thermal desorption particle beam mass spectrometer. *Environmental Science and Technology,* 35: 2233–2243.

Chapter 4: Effects of Transient Valve Timing on Particulate Emissions

It is important to consider particle emissions from HCCI engines because automotive particle emissions are regulated. Diesel engine particle mass has long been regulated, however, Euro 5/6 standards introduced particle number regulations for diesel vehicles, as well as particle mass regulations for gasoline vehicles. Beginning in 2014, particle emission number regulations will also be applied to gasoline vehicles (European Commission, 2007).

In automotive applications, the engine speed and load often change quickly to accommodate the demands of the driver. To understand the particle emissions from HCCI engine operation, it is important to consider the effect that changing engine operating conditions has on particle size and concentration. To be able to observe these transitory effects, it is necessary to measure the particle emissions with fast-response equipment. Previous work has been done to measure the steady-state particle emissions from gasoline HCCI engines (Section 1.2; Makato, 2001; Yamane, 2002; Peng, 2005), but no work reported on the transient particle emissions.

4.1 Transient Testing Configuration

A single-cylinder Ricardo experimental engine with fully-variable electromagnetic valves as described by Seethaler (2013) is used. The valves allow cycle-by-cycle switching of the engine operating conditions. The engine is operated at approximately 820 rpm (7 cycles/s) with valve timings of both 60° and 180° of symmetric negative valve overlap (NVO) (Ebrahimi, 2013). NVO causes the exhaust valve to close before the intake valve is opened. To increase the NVO, the exhaust valve closing timing is advanced and the intake valve opening time is retarded. This causes more hot residual gases to be trapped, which advances the combustion timing and the peak combustion pressure. Cylinder pressure traces as a function of crank angle for both operating conditions are shown in Figure 4.1.

A fast-response DMS is used to measure the particle emissions created during engine operation. The DMS measured the particle size distribution from which the total particle concentration can be calculated. The DMS has a response time of 500 ms (which is on the same order as the engine speed) and the sampling rate is set to 2 Hz. Engine exhaust is sampled immediately downstream of the exhaust valve to reduce particle losses due to diffusion or thermophoretic deposition. The sampling line uses a line controller to dilute the mixture at the sampling head by a ratio of 5 and to heat the exhaust gases to 70°C. This prevents diffusion and thermophoretic deposition, as well as particle formation through nucleation or accumulation. Once the exhaust gases reach the DMS, they are further diluted by a ratio of 6 before being sampled, which gives a cumulative dilution of 30 (except during the 60° NVO steady-state test where the second stage dilution is set to 1).

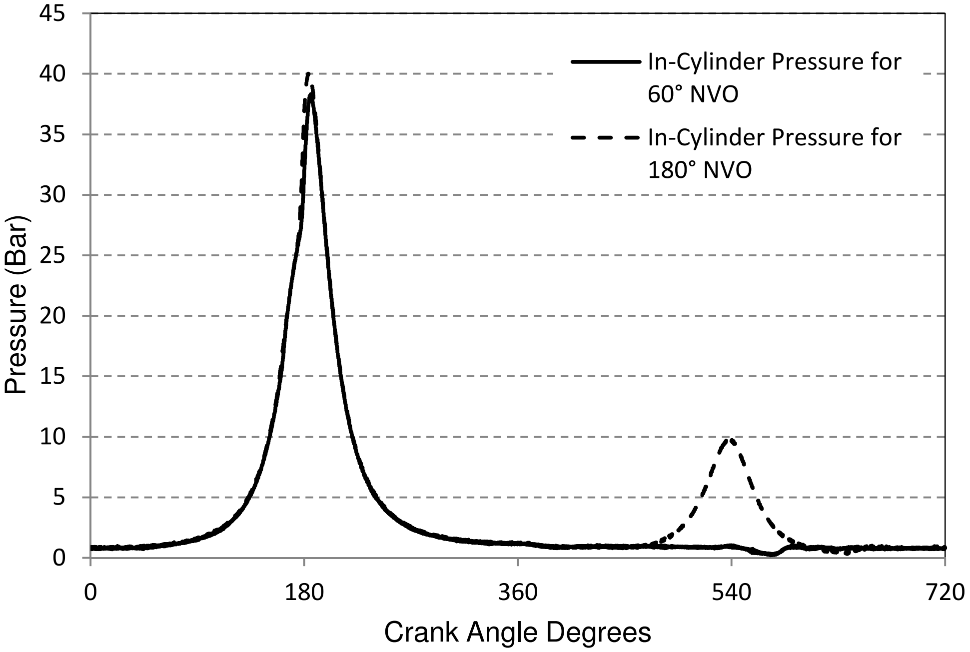

Figure 4.1: Representative in-cylinder pressure trace for HCCI combustion with 60° and 180° NVO.

4.2 Results

To establish the baseline particle emissions, the differential mobility spectrometer (DMS) is first used to measure the steady-state particle emissions for both 60° and 180° of NVO. The operating conditions and PM data collected with the DMS is summarized in Table 4-1. The average particle distribution for 60° and 180° NVO are shown in Figure 4.2. For 60° NVO the geometric mean diameter (GMD) is 15.1 ± 1.5 nm with a geometric standard deviation (GSD) of 1.56. The average particle concentration is $6.0\text{x}10^7$ ± $1.7\text{x}10^7$ cm^{-3} (all uncertainties are given with 95% confidence). For 180° NVO the GMD is 16.0 ± 1.6 nm with a GSD of 1.51. The average particle concentration is $5.7\text{x}10^7$ ± $1.8\text{x}10^7$ cm^{-3}. Operating at both 60° and 180° NVO results in similar particle distributions and total number concentration. These two operating points also agree well within the uncertainty of the instrument.

Table 4-1: Engine and PM parameters for steady-state conditions. Particulate number (N) and mass (M) include both volatile and non-volatile particles. Particle density is assumed to be 850 kg/m^3, based on section 3.2.3.

Mode	CR	NVO	IMEP (bar)	Φ	GMD (nm)	GSD	N (cm^{-3})	M (g/cm^3)
HCCI	12	60	2.07	0.26	15.1	1.56	6.0E+7	2.2E-10
HCCI	12	180	2.11	0.42	16.0	1.51	5.7E+7	2.2E-10

After establishing the steady-state particle emissions for both 60° and 180° NVO, the DMS is used to record measured particle emissions while the valve timing is repeatedly changed back and forth between 60° and 180° NVO. It is important that the particle emissions are observed for a random selection of cycles to give a representative measurement of all engine cycles. This is achieved by switching back and forth between the two operating points a large number of times at random intervals. A pseudo random binary signal (PRBS) is used to switch between valve timings. This signal randomly excites the system (i.e. the engine) over a wide range of frequencies. This ensures a change in engine operation is due to the valve timing change and not a result of a natural engine frequency.

The total particle concentration measured by the DMS during the transient test, as well as the time-averaged total particle concentration for the steady-state tests at 60° and 180° NVO are shown in Figure 4.3 for comparison. The valve overlap used during the transient test is also shown. Synchronizing (in time) the particle concentration measurements with the valve timing for each cycle, it is apparent that there is a close correlation between the peaks in particle concentration and the timing changes. Specifically, the spike in particulate concentration correlates with the change from 180° NVO to 60° NVO. However, because the DMS sampling rate is lower than the engine cycle rate, not every timing change event resulted in a visible spike in particle concentration. The particle concentration between spikes is at similar levels to the steady state operation; whereas, the spikes observed in particle concentration due to a valve timing change increase by nearly an order of magnitude. The highest concentration observed was approximately 2.7 x10^8 cm^{-3}, however, the time-response limitation of the DMS (500 ms) means that the particle concentration would be attenuated, and because of the sampling rate (2 Hz), the maximum could be missed. Thus, the actual maximum particle concentration corresponding to a change in valve timing is expected to be greater than the measured value.

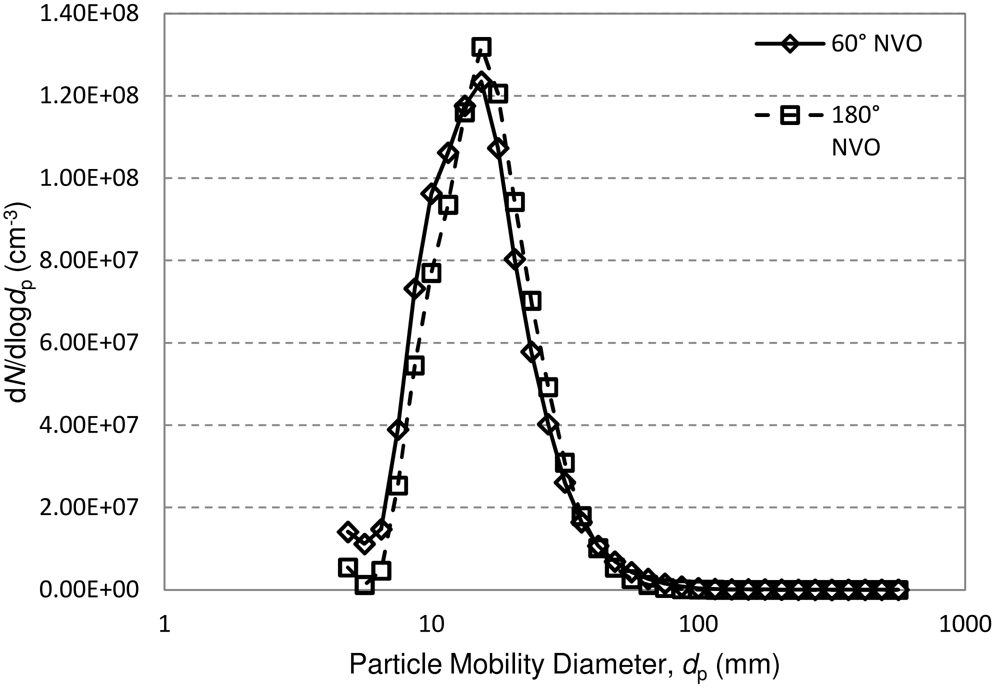

Figure 4.2: Particle distribution for steady-state 60° and 180° NVO.

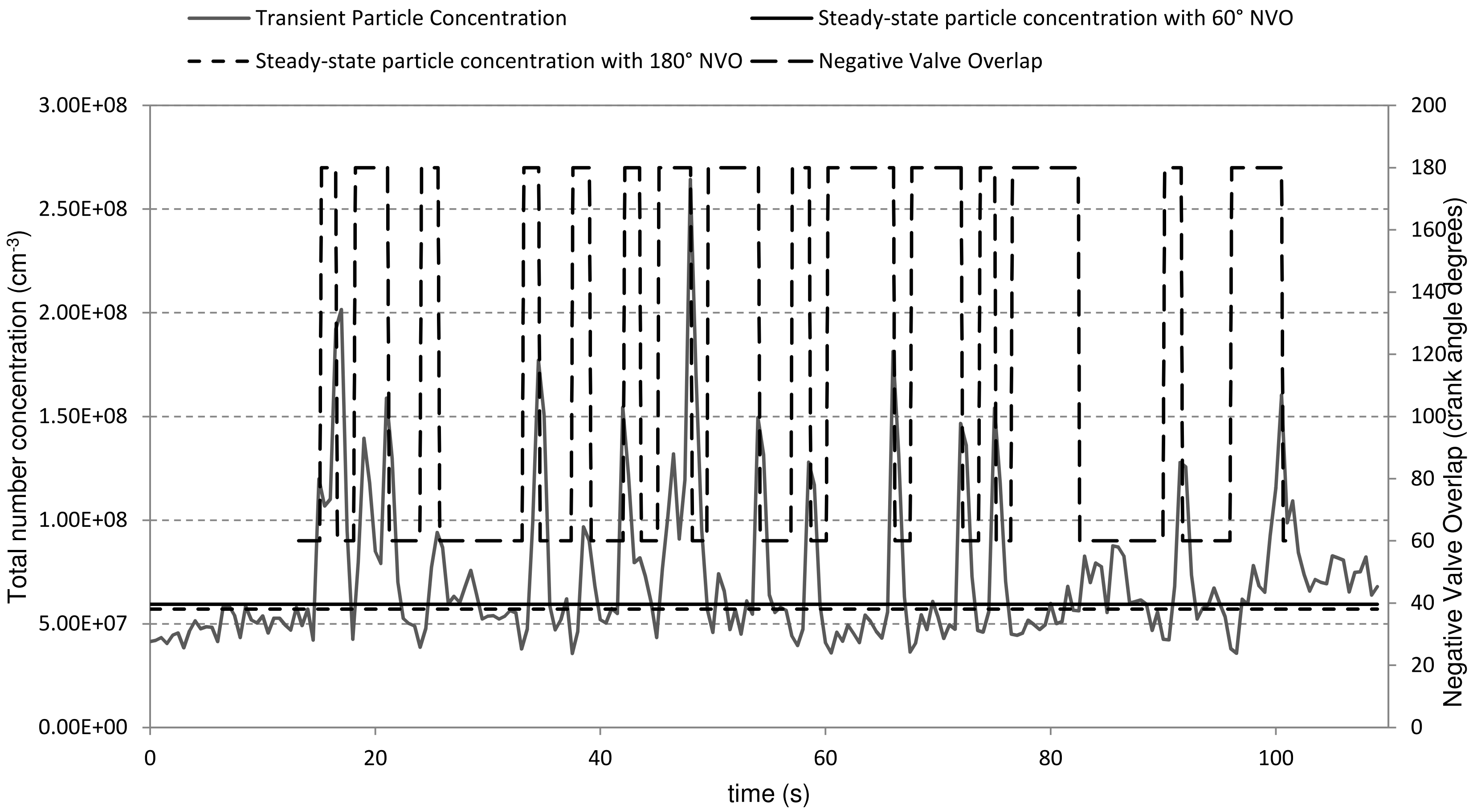

Figure 4.3: Particle concentration measured during transient engine operation. Steady-state particle concentrations recorded at 60° and 180° NVO are also shown, but are not a function of time and are included only for comparison. NVO is also shown and corresponds to the secondary *y*-axis.

While using a DMS allows for fast measurements of transient particle distribution, it would also be useful to measure the mass or number concentration in an integrated fashion to quantify the magnitude of the increase in emissions under these transient conditions. For example, the integrated mass concentration could be measured with filter measurements, but this has not yet been done.

The particle size distribution measured during transient operation is shown in Figure 4.4. This figure graphically depicts the particle concentration peaks due to valve timing changes. While the particle concentration spikes as a result of changing operating conditions, the GMD and GSD remain fairly constant. The GMD remains at 15 ± 1.5 nm throughout the test. Also, the size distribution remains unimodal. This suggests that the mechanism for particle formation remains the same, whereas the presence of larger particles would suggest the formation of new types of particles, like soot. The previous steady-state experiments (Chapter 3) resulted in similar size distributions and volatility experiments suggested that the particles are likely composed of unburnt lubricating oil. Therefore, it is likely that the particles generated by this engine are also lubricating oil. However, this was not tested because the volatility experiments require long sampling times.

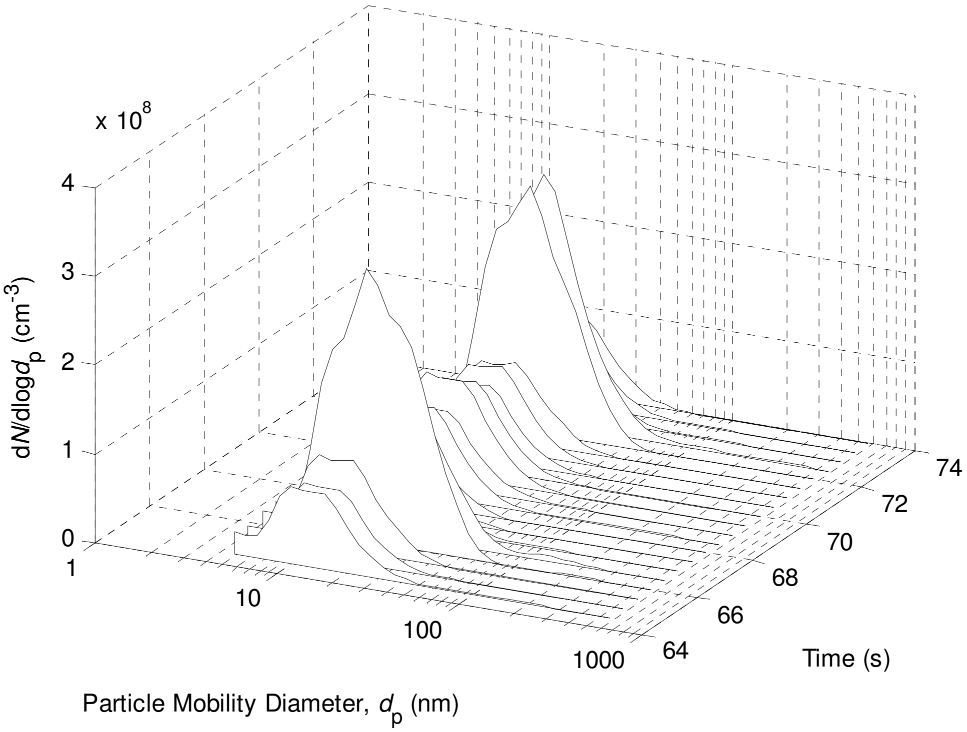

Figure 4.4: Size distributions from transient measurements showing concentration spikes due to changing operating conditions.

4.3 Conclusions

HCCI engines in automotive applications are constantly required to change loads and speeds due to driver commands. To quantify the particle emissions produced in HCCI combustion, a fast-response DMS is used to measure the particle concentration and size distribution during steady state and transient engine operation. Electromagnetic valves that allow for cycle-by-cycle valve changes are used in a symmetric NVO strategy, which results in nearly an order of magnitude spike in particle concentration. These transient changes in PM emissions triggered by valve timing changes from 180° NVO to 60° NVO are followed by a quick return to steady-state levels. The size distribution indicates that, while the concentration increased, the distribution remains quite similar. This suggests that the mechanism for particle formation remains the same. Previous work with steady state volatility testing indicates that the particulate emissions are volatile and are mostly composed of engine oil.

4.4 References

Ebrahimi, K., Schramm, A., Koch, C. R. (2013). A control oriented model with variable valve timing for HCCI combustion timing control. *SAE Technical Paper Series*, 2013-01-0588.

European Commission. (2007). Regulation No 715 of the European Parliament and of the council of 20 June 2007 on type approval of motor vehicles with respect to emissions from light passenger and commercial vehicles (Euro 5 and Euro 6) and on access to vehicle repair and maintenance information. (2007). *Official Journal of the European Union*.

Makoto, K., Koji, M., Jin, I., Yohei, S. (2001). Study on homogeneous charge compression ignition gasoline engine. *Subaru Technical Review*, 28:89-96.

Peng, Z., Zhao, H., Ma, T. (2005). Characteristics of homogeneous charge compression ignition (HCCI) combustion and emissions of n-heptane. *Combustion Science and Technology*, 177(11).

Seethaler, R., Mashkournia, M., Chladny, R. R., Zhao, J., Koch, C. R. (2013). Closed loop electromagnetic valve actuation motion control on a single cylinder engine. *SAE Technical Paper Series*, 2013-01-0594.

Yamane, K., Shimamoto, Y. (2002). Combustion and emission characteristics of direct-injection compression ignition engines by means of two-stage split and early fuel injection. *Journal of Engineering for Gas Turbines and Power*, 124(3):660-667.

Chapter 5: Conclusion

By using a single cylinder CFR engine, steady state particulate emissions properties are studied during motoring, SI, and HCCI operation. Motoring and SI operation at low and high compression ratios show that an increasing compression ratio results in a higher particle concentration, as well as a larger GMD. The engine can only operate in HCCI at a high compression ratio, where it produces particle concentrations similar to that of motoring and SI at high compression ratio. The high compression ratio seems to result in more volatile compounds distilling from the engine oil. In comparison to SI and HCCI operation, motoring produces a higher concentration of PM, and also results in a larger GMD, which suggests that some of the volatile material is being combusted.

Thermodenuder tests show that at a temperature of 100 °C, less than 5% of the PM volume fraction remains for all operating conditions, with further PM evaporating at higher temperatures, suggesting that the engine oil is the primary component. The effective density of the PM during motoring, SI, and HCCI operation is fairly constant at approximately 850 kg/m^3 over a range of particle sizes, which is a reasonable density for engine oil.

Using a single cylinder engine with electromagnetic valves, the PM emissions are measured during transient HCCI engine operation. Switching the valve timing from 180° NVO to 60° NVO causes a transient increase in PM concentration by nearly an order of magnitude, which coincides with the valve timing change. After a sharp increase in PM concentration, there is a quick return to steady state levels. The GMD remains nearly unchanging. The conclusion can be made that while the PM concentration increases, the similar size distribution suggests that the mechanism for particle formation does not.

Therefore the PM produced during transient HCCI is also primarily composed of engine oil distillates.

Appendix A: Uncertainty Analysis

Measured values and true values are not the same. The difference between these values is defined as error, and all measurements involve some amount of error. This error can be estimated by calculating the uncertainty. Uncertainty has two sources. The first source of uncertainty is precision uncertainty, which results from error when making the measurement. This can be estimated by performing repeated measurements and is represented by P_x. The second is bias uncertainty, which is the systematic uncertainty resulting from the measurement instrument used. Bias uncertainty must be estimated from other sources, and is often reported by the equipment manufacturer. This type of uncertainty is represented by B_x. These two types of uncertainty can be combined to determine the total uncertainty, U_x. It can be calculated with the following equation.

$$U_x = \sqrt{\sum B_x^2 + P_x^2}$$

To estimate the precision uncertainty, multiple measurements are made, and the value is calculated by:

$$P_x = t_{\frac{\alpha}{2},v} \frac{S_x}{\sqrt{n}}$$

$\alpha = 1 - c$, where c is the confidence interval used (usually 95%), and $v = n - 1$, which is the degrees of freedom. The values for the t-distribution are tabulated. S_x is the standard deviation, and n is the number of measurements made.

The values for bias uncertainty used in the calculations for this work are shown in Table A-1.

Table A-1: Reported bias uncertainties for equipment measurements.

Instrument	Parameter	Bias Uncertainty
DMA (Mulholland, 1999)	Mobility Diameter of Particles	3%
CPC (TSI, 2012)	Particle Concentration	10%
CPMA (Symonds, 2012)	Particle Mass	2.8%
DMA-CPMA	Particle Density	9.4%
DMS (Symonds, 2010)	Mobility Diameter of Particles	10%
DMS w/ primary & secondary dilution (Symonds, 2010)	Particle Concentration	32%
DMS w/ secondary dilution (Symonds, 2010)	Particle Concentration	28%

In order to obtain the bias uncertainty for the particle density measured with a DMA-CPMA system, the bias uncertainty of the individual instruments must be combined. The particle density is proportional to m/d^3, and since the CPMA has an uncertainty in mass of 2.8%, and the DMA has an uncertainty in diameter of 3%, through the propagation of error, we obtain an uncertainty of 9.4% for the density of a particle measured with a DMA-CPMA system. The related equation is:

$$\frac{\varepsilon_\rho}{\rho} = \sqrt{\left(\frac{\varepsilon_m}{m}\right)^2 + 3^2\left(\frac{\varepsilon_d}{d}\right)^2}$$

A.1 References

Mulholland, G., Bryner, N., Croarkin, C. (1999). Measurement of the 100 nm NIST SRM 1963 by differential mobility analysis. *Aerosol Science and Technology,* 31(1): 39–55.

Symonds, J. (2010). *Calibration of fast response differential mobility spectrometers*. National Physical Laboratory (NPL), London, UK: Metrology of Airborne Nanoparticles, Standardisation and Applications (MANSA).

Symonds, J., Reavell, K., Rushton, M., Lowndes, C. (2012). *The centrifugal particle mass analyser as a fundamental particle mass standard.* Cambridge, UK: Cambridge Particle Meeting.

TSI. (2012). Ultrafine Condensation Particle Counter Model 3776. Retrieved 3 Sep. 2013.
http://www.tsi.com/uploadedFiles/_Site_Root/Products/Literature/Spec_Sheets/3776_2980345.pdf